CHROMOPHORE ROTATIONAL DYNAMICS AS A PROBE OF LOCAL ORGANIZATION IN BULK AND INTERFACIAL SYSTEMS

By

Hannah Mize

A THESIS

Submitted to
Michigan State University
in partial fulfillment of the requirements
for the degree of

Chemistry-Master of Science

2017

ABSTRACT

CHROMOPHORE ROTATIONAL DYNAMICS AS A PROBE OF LOCAL ORGANIZATION IN BULK AND INTERFACIAL SYSTEMS

By

Hannah Mize

The use of chromophore rotational motion to study local organization is well established. Under certain conditions, the same measurements can be used to evaluate the effect(s) of thermal energy transfer from the chromophore to the bath. Such information is of central importance to gaining a fundamental understanding of the intermolecular interactions that are ultimately responsible for bulk system properties, and to the creation of biomimetic mono- and bilayer structures. This thesis includes studies that address each of these areas.

The first study, focusing on understanding the molecular scale consequences of thermal energy dissipation in bulk systems, reports on the rotational diffusion dynamics of tetracene in a series of n-alkane solvents, where differences in those dynamics were measured for excitation to the S1 and S2 states. These data demonstrated that for excitation to the S2 state, fast non-radiative relaxation to the S1 state produces transient heating of the solvent surrounding the chromophore, with the details depending on the identity of the solvent bath.

The second study aims at understanding the influence of the aqueous overlayer in contact with a planar bilayer on molecular scale organization and phase separation. These data reveal organization-dependent changes in the bilayer that depend on both the pH and the ionic strength of the aqueous overlayer. These findings are of direct relevance to the use of such films in the construction of biomimetic sensors, for example, where organization is expected to influence the ability of the bilayer to host biomolecules in their active forms and to mediate permeability.

ACKNOWLEDGEMENTS

I would like to thank all members of the Blanchard group at Michigan State University: Christine Hay, Iwan Setiawan, Chen Qiu, Fredy Pratama, Stephen Baumler, Xiaoran Zhang, Krystyna Kijewska, Ke Ma, Barrack Stubbs, Cameron Meyer, Andrew McHale and Jillian Mutchler. Working with them has been a pleasure and they have helped me and supported me every step of the way through my graduate degree. I will never forget my time in the Blanchard group thanks to all of the fun memories.

My family has been very supporting throughout my undergraduate and graduate education: George and Leola Mize, Kellie and DJ Jones, Rebekah and Canton Brissette. They were always there for advice. They guided me through the process of reaching my full potential and realizing what type of career would make me most happy.

I am incredibly thankful to Dr. Gary Blanchard for being my advisor during my time in the Michigan State Chemistry Department. Dr. Blanchard is far more than an advisor, he goes above and beyond for the students in his group. He not only shares his vast knowledge and helps us develop our research skills, he also inspires us to be the best version of ourselves. Graduate school can be a new and difficult process for some students, and every student is different. It is amazing to see how he connects with each student individually and always has his door open to help. Not only do I owe my success in graduate school to him, I also appreciate how much he has helped me grow as a person. He has inspired me to go out into the world and build my life around a passionate career, not just one that was expected of me.

I am very grateful to Dr. David Karpovich for mentoring me as an undergraduate at

Saginaw Valley State University. Without him, I would not have been introduced to research or gone to graduate school. It has been an amazing adventure, filled with self-discovery, and at the end I have a clear understanding of what God is calling me to do.

I am very thankful for the GAANN program for providing me with assistance throughout my graduate education.

TABLE OF CONTENTS

LIST OF TABLES

LIST OF FIGURES

CHAPTER 1

Background and Motivation

Introduction

Intermolecular interactions play a substantial, often deterministic role in the material and functional properties of essentially all chemical systems. Consequently, it is important to determine how dissimilar molecules interact with one another, from both steric and energetic perspectives. Spectroscopy is a well established means of characterizing intermolecular interactions in both bulk and interfacial systems, and depending on the system of interest, a probe chromophore is used for such measurements.

This thesis is concerned with the use of fluorescent probe molecules to interrogate selected local environments. The systems chosen for study were deliberate. In the first study, the chromophore tetracene was dissolved in bulk n-alkane solvents n-octane through n-hexadecane, and the issues of interest were what effect solvent molecular size has on the motion of the chromophore, and how efficiently thermal energy is dissipated in such systems. Our data demonstrated that the dissipation of thermal energy in the n-alkanes exhibits an odd-even effect for longer n-alkanes, a finding that implicates the terminal methyl groups of the solvent as playing a mediating role in thermal energy dissipation.

In a second body of work, the focus was a planar supported lipid bilayer containing three constituents; a phosphocholine, sphingomyelin and cholesterol, and the probe chromophore was tethered to a phosphoethanolamine moiety for integration into the bilayer. In this work the external variable of interest was not thermal energy, but the composition of the aqueous

overlayer in contact with the supported bilayer. Our data demonstrated that the local environment experienced by the chromophore depended on overlayer pH and ionic strength, and we can understand certain of these dependencies on ionic screening effects. In addition, imaging data revealed that the morphology of the supported bilayer (phase separation of the phosphocholine and cholesterol components) also depended on the pH and ionic strength of the aqueous overlayer.

While the chemical systems chosen for study are quite different, the larger result is that the chemical composition and organization of the environment in the immediate proximity of the chromophore determines the properties sensed by the chromophore in a predictable manner. In Chapters 2 and 3 of this thesis, these studies are discussed in detail.

Despite the chemical and physical differences between the systems studied, the technology used to examine them was similar and the underlying physics that describe chromophore molecular motion are similar. In this thesis we prioritize the chemical information content in Chapters 2 and 3 and provide a discussion of the measurements and data interpretation in Chapter 1, below.

Over a wide range of sample formats the most effective means of characterizing chromophore molecular motion is through fluorescence depolarization measurements. Such measurements can be performed either in the steady state or using time-resolved spectroscopic techniques. The former requires assumptions about the fluorescence lifetime and the chromophore local environment in order to interpret the data. The latter, time-resolved detection of polarized emission transients, provides the most useful data in terms of information content and there exists a well established theoretical framework for data interpretation. This is the means by which the data reported in this thesis were acquired.

There are a variety of ways to acquire time-resolved data, with the ability to detect chromophore motion in the S_0 (ground state), S_1 (first excited singlet state) or higher excited states. Detection of chromophore motion in the S_0 ensures that no excess spectroscopic energy that is dissipated nonradiatively contributes to local heating. Such measurements detect ground state recovery and require a two-laser pump-probe configuration. While the sensitivity of such measurements can be high (shot noise limited), the implementation of such a system is complex and time-consuming. For the measurement of anisotropy decay dynamics from the chromophore S1 or higher excited electronic states, time-resolved fluorescence detection is typically used. While this detection method does not provide quite as high time resolution as pump-probe measurements, it does offer much greater versatility in terms of sample format and optical collection of the relevant signal. In this work, time-correlated single photon counting (TCSPC) detection technology is used for the collection of all time-domain spectroscopic data.

TCSPC detection requires the use of a polarized pulse of light to excite the sample, preferably with the duration of the excitation pulse being short relative to the timescale on which chromophore molecular motion proceeds. The TCSPC systems in use in the Blanchard group use synchronously pumped, cavity dumped dye lasers to produce pulses of 5 ps duration (FWHM). At times short after excitation, the polarization-selected ensemble of excited molecules exhibits an orientational distribution that is not random, and where most of the excited chromophores are oriented parallel to the polarization of the excitation pulse. Monitoring of fluorescence from this ensemble at polarizations parallel and perpendicular to the excitation polarization shows that initially the fluorescence polarized parallel to the excitation pulse is more intense than that polarized perpendicular to the excitation pulse (assuming the excited and emitting transition moments re parallel. The opposite obtains if the transition moments are

perpendicular and this point is considered in detail in Chapter 2). With increasing time after excitation, the polarized emission components become the same intensity as the initial anisotropic population or excited chromophores re-randomizes to produce a random orientational distribution. The timescale and functional form of this relaxation process can be quantitated and related to the properties of the chromophore local environment.

Chuang and Eisenthal have treated this problem experimentally for a free rotor, which is appropriate for solution phase measurements (Chapter 2). They describe the polarized emission transients $I_{\|}(t)$ an $I_{\perp}(t)$ as a function of the Cartesian components of the rotational diffusion constant, D, and the orientations of the excited and emitting transition dipole moments, γ and q.

$$I_{\mathrm{P}}(t) = P(t)\left\{\begin{array}{l} \frac{1}{9} + \frac{4}{15} q_x q_y \gamma_x \gamma_y \exp\left(-3\left(D_z + D\right)t\right) \\ + \frac{4}{15} q_y q_z \gamma_y \gamma_z \exp\left(-3\left(D_x + D\right)t\right) \\ + \frac{4}{15} q_z q_x \gamma_z \gamma_x \exp\left(-3\left(D_y + D\right)t\right) \\ + \frac{1}{15}\left(\beta + \alpha\right)\exp\left(-\left(6D + 2\Delta\right)t\right) \\ + \frac{1}{15}\left(\beta - \alpha\right)\exp\left(-\left(6D - 2\Delta\right)t\right) \end{array}\right\} \qquad [1.1]$$

$$I_{\perp}(t) = \tfrac{1}{6} P(t) - \tfrac{1}{2} I_{\mathrm{P}}(t)$$

Where P(t) is the radiative population decay of the ensemble, $P(t) = \exp(-t/\tau_{fl})$ τ_{fl} = fluorescence lifetime) and the terms in Eq. 1 are given by

$$1 = q_x^2 + q_y^2 + q_z^2$$

$$1 = \gamma_x^2 + \gamma_y^2 + \gamma_z^2$$

$$\beta = \left(q_x^2\gamma_x^2 + q_y^2\gamma_y^2 + q_z^2\gamma_z^2 - \tfrac{1}{3}\right)$$

$$\alpha = \left\{\begin{array}{l} \left(\frac{D_x}{\Delta}\right)\left(q_y^2\gamma_y^2 + q_z^2\gamma_z^2 - 2q_x^2\gamma_x^2 + \gamma_x^2 + q_x^2\right) + \\ \left(\frac{D_y}{\Delta}\right)\left(q_z^2\gamma_z^2 + q_x^2\gamma_x^2 - 2q_y^2\gamma_y^2 + \gamma_y^2 + q_y^2\right) + \\ \left(\frac{D_z}{\Delta}\right)\left(q_x^2\gamma_x^2 + q_y^2\gamma_y^2 - 2q_z^2\gamma_z^2 + \gamma_z^2 + q_z^2\right) - \\ \left(\frac{2D}{\Delta}\right) \end{array}\right\} \qquad [1.2]$$

$$D = \tfrac{1}{3}\left(D_x + D_y + D_z\right)$$

$$\Delta = (D_x^2 + D_y^2 + D_z^2 - D_xD_y - D_yD_z - D_zD_x)^{1/2}$$

The terms α, β and D are all related to the anisotropy of the molecular motion. The polarized fluorescence transients (schematized in Fig. 1.1) are permuted to form the anisotropy decay function, R(t).

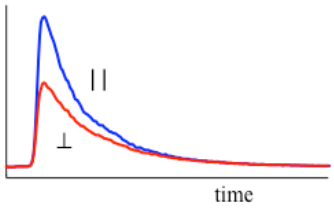

Figure 1.1 Schematic depiction of the polarized emission transients parallel and perpendicular to the polarized excitation pulse.

$$R(t) = \frac{I_{\mathrm{P}}(t) - I_{\perp}(t)}{I_{\mathrm{P}}(t) + 2I_{\perp}(t)} \qquad [1.3]$$

Incorporation of Eqs. 1.2 into 1.3 gives

$$R(t) = \begin{Bmatrix} \frac{6}{5} q_x q_y \gamma_x \gamma_y \exp\left(-3\left(D_z + D\right)t\right) + \\ \frac{6}{5} q_y q_z \gamma_y \gamma_z \exp\left(-3\left(D_x + D\right)t\right) + \\ \frac{6}{5} q_z q_x \gamma_z \gamma_x \exp\left(-3\left(D_y + D\right)t\right) + \\ \frac{3}{10}\left(\beta + \alpha\right)\exp\left(-\left(6D + 2\Delta\right)t\right) + \\ \frac{3}{10}\left(\beta - \alpha\right)\exp\left(-\left(6D - 2\Delta\right)t\right) \end{Bmatrix}. \qquad [1.4]$$

While R(t) can contain up to five exponential decay components, the astute choice of coordinate system such that the excited and emitting transition moments lie along Cartesian axes simplifies R(t) to contain at most two decay components.

$$R(t) = \tfrac{3}{10}(\beta + \alpha)\exp\left(-(6D + 2\Delta)t\right) + \tfrac{3}{10}(\beta - \alpha)\exp\left(-(6D - 2\Delta)t\right) \qquad [1.5]$$

The terms α and β (Eqs. 1.2) are determined by the orientation(s) of the excited and emitting transition dipole moments, with the resulting equations given in Chapter 2.

The functional form of R(t) allows for the extraction of at least some Cartesian components of D, and it is the relationship between D and system properties that is of interest. For the simplest and most frequently encountered case,

$$R(t) = \tfrac{2}{5}\exp(-t/\tau_{OR}) \qquad [1.6]$$

With τ_{OR}, the orientational relaxation time constant being related to system properties according to the modified Debye-Stokes-Einstein equation,[1-4]

$$\tau_{OR} = \frac{1}{6D} = \frac{\eta V f}{k_B T S} \qquad [1.7]$$

where η is the solvent bulk viscosity, V is the solute (chromophore) hydrodynamic volume, *f* is a term to describe frictional intermolecular interactions, and *S* is a term to account for the ellipsoidal shape of solute. It is typically held that the rotating chromophore sweeps out an ellipsoidal volume as it rotates, and the factor that determines whether one decay component or two is seen is the dominant rotational axis relationship to the axis or axes along which the

transition dipole moment lies. Two rotor shapes can be considered (assumes x-axis polarization of the transition moments): oblate ($D_z > D_x = D_y$) and prolate ($D_x > D_y = D_z$) (Figure 1.6).[5] Under these conditions, a prolate rotor would yield a one-component exponential decay because the transition moment axis is coincident with the dominant rotational axis, and only rotational motion perpendicular to the polarization axis ($D_y = D_z$) will be observable. An oblate rotor would exhibit a two component anisotropy decay because there are two unique rotational axes perpendicular to the transition moment axis ($D_y \neq D_z$).

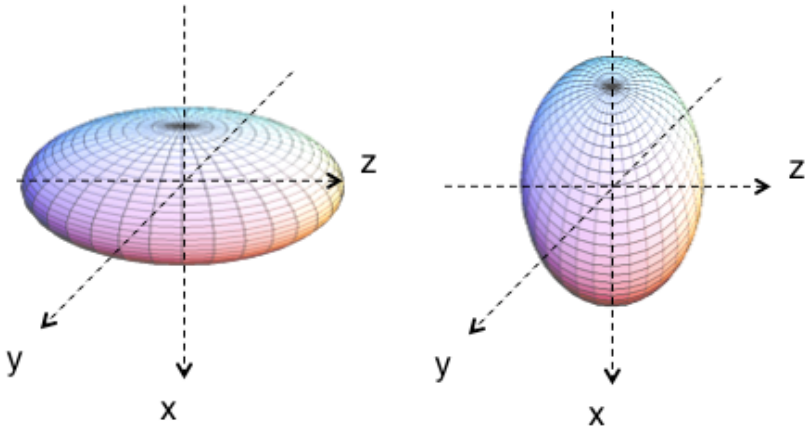

Figure 1.2 As a molecule rotates around the axis of rotation, it can have an oblate (left) or a prolate (right) rotor shape.

The work described in Chapter 2 relates to a free rotor, as described above. The work described in Chapter 3 makes use of a chromophore that is tethered to a nominally planar interfacial bilayer structure. For such systems, the same polarized emission transients are acquired and used to produce the induced orientational anisotropy function, R(t), (Eq. 1.3). Interpretation of the functional form of R(t) for a tethered chromophore is described in the context of the so-called Hindered Rotor model. The physical basis for this model is that the chromophore is free to execute random motion as limited by its tethering bond, described by a

"wobbling" diffusion constant, Dw. It is not appropriate to describe this diffusion constant as exactly the same as that for the free rotor because the wobbling motion of the tethered chromophore is itself constrained by the tether. In addition to this diffusional wobbling motion, the chromophore-tether molecule can relax into some orientational distribution that is determined by the constraints imposed on it by the surrounding interface constituents. This limited orientational distribution is modeled as a cone of semi-angle θ_0 (Fig. 1.7).

Because the orientational distribution of chromophores is not free to relax into all orientations, the function R(t) may possess an infinite time component, the value of which is related to the cone semi-angle, θ_0,

$$\theta_0 = \cos^{-1}\left(\tfrac{1}{2}\left(8\left(\frac{R(\infty)}{R(0)}\right)^{1/2}+1\right)^{1/2}-\tfrac{1}{2}\right) \qquad [1.8]$$

As the R(t) decays from its zero-time value (R(0), related to the angle between the absorbing and emitting transition moments) and its infinite-time value, R(∞), the time constant for that decay is given by

$$\tau_{HR} = \frac{7\theta_0^2}{24D_w} \qquad [1.9]$$

It is the quantity D_w that is related most directly to the chromophore local environment.[6]

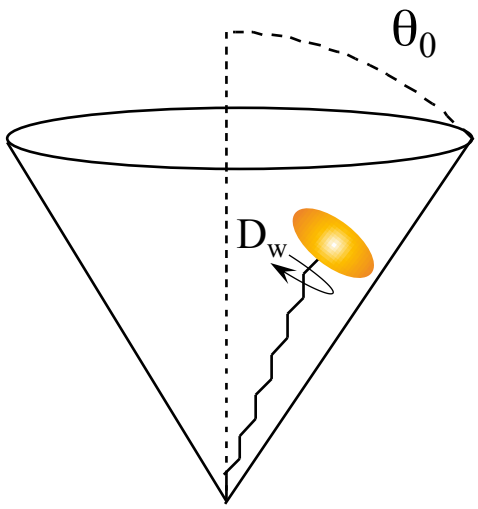

Figure 1.3 Schematic of the confining cone described by the hindered rotor model, where θ_0 is the cone semi-angle and D_w is the diffusion constant describing motion of the chromophore about its tethering bond.

Conclusions

The characterization of chromophore molecular motion, both in bulk and at interfaces, can be understood within the context of well established models. Specific limiting cases of these models will be applied to the treatment of the data presented in Chapters 2 and 3 to provide molecular-scale insight into the local environment of the chromophores. Taken collectively, these illustrative studies provide insight into intermolecular interactions and how they can be examined using time-resolved spectroscopic methods.

REFERENCES

REFERENCES

1. Debye, P., Polar Molecules Chemical Catalog Co.: New York **1929**; p 84.

2. Chuang, T. J.; Eisenthal, K. B., Theory of fluorescence depolarization by anisotropic rotational diffusion. *Journal of Chemical Physics* **1972,** *57* (12), 5094-5097.

3. Perrin, F., Mouvement brownien d'un ellipsoide (I). Dispersion dielectrique pour les molecules ellipsoidale. *Le Journal de Physique et le Radium* **1934,** *5*, 497.

4. Perrin, F., Mouvement Brownien d'un ellipsoide (II). Rotation libre et depolarisation des fluorescences. Translation et diffusion de molecules ellipsoidales. *Le Journal de Physique et le Radium* **1936** *7*,1-11.

5. DelaCruz, J. L.; Blanchard, G. J., Reorientation Dynamics of Rhodamine 640 in Normal Alcohols. Measurement of the Length and Time Scale of Transient Local Heating in Solution, *J. Phys. Chem. A*. **2001**, *105*, 9328-9335.

6. Lipari, G.; Szabo, A., Effect of Librational Motion on Fluorescence Depolarization and Nuclear Magnetic Resonance Relaxation in Macromolecules and Membranes. *Biophys. J.* **1980,** *30*, 489-506.

CHAPTER 2

State-dependent rotational diffusion of tetracene in n-alkanes. Evidence for a dominant energy relaxation pathway

This chapter is adapted from Hannah E. Mize and G. J. Blanchard, "State-Dependent Rotational Diffusion of Tetracene in *n*-Alkanes. Evidence for a Dominant Energy Relaxation Pathway," *Journal of Physical Chemistry B*, **117**, 16260-16265 (2013).

Introduction

Understanding the flow of energy between molecules is the fundamental first step toward elucidating the molecular basis for thermal conductivity. There have been a number of efforts aimed at modeling thermal conductivity phenomenologically,[1-3] but limited investigation of intermolecular vibrational energy transfer.[4-11] Understanding and characterizing the details of intermolecular energy transfer in fluid systems can be challenging from an experimental standpoint because the transfer of energy between specific vibrational modes of one molecule and the vibrational, rotational and translational degrees of freedom of the bath molecule(s) depends on a number of physical, spectroscopic, and geometric factors.[12-21] A comparatively straightforward means of monitoring vibrational energy transfer is with an experiment that senses the transient temperature change of a molecule's immediate environment following the dissipation of a pre-determined amount of energy by nonradiative means. Using this method we have characterized the effect of transient heating on chromophores.[22-24] We have found that in polar or amphiphilic systems the transient temperature change sensed by these measurements is modest, on the order of several K.

We are interested in understanding the effects of transient heating on local organization. In an earlier work, which focused on quantitating the transfer of vibrational energy between specific tetracene normal modes and those of surrounding *n*-alkane solvents, we found evidence

for relatively facile relaxation, and one possible explanation for these findings was that the tetracene chromophore was acting as a template for the organization of solvent molecules in its immediate proximity.[10] In an effort to understand these results in greater detail, we have examined tetracene in the *n*-alkanes octane through hexadecane, comparing the reorientation dynamics of this chromophore in each alkane under conditions of $S_1 \leftarrow S_0$ and $S_2 \leftarrow S_0$ excitation. These experiments have revealed a number of interesting points, including a comparatively large transient heating effect and the existence of a pronounced odd-even solvent effect that is seen in both chromophore dynamics and solvent thermal energy dissipation. These findings support the role of tetracene in providing a structural template for the organization of solvent molecules in close proximity.

Experimental Methods

Chemicals. Tetracene (98%) and the n-alkanes octane (99%), nonane (99%), decane (99%), undecane (99%), dodecane (99%), tridecane (99%), tetradecane (99%), pentadecane (99%) and hexadecane (99%) were purchased from Sigma-Aldrich and used without further purification.

Time-resolved fluorescence measurements. Time-domain fluorescence lifetime and anisotropy decay data were acquired using a time-correlated single photon counting instrument that has been described in detail previously,[23] and we recap only its essential features here. Briefly, the sample is excited by linearly polarized 5 ps pulses of light that are generated by a synchronously pumped cavity dumped dye laser (Coherent 702, Gooch and Housego cavity dumping electronics). The source laser is a passively mode locked Nd:YVO_4 diode pumped laser (Spectra Physics Vanguard) that produces 13 ps pulses at 80 MHz repetition rate. The output of this laser is 2.5 W average power at 355 nm and 2.5 W average power at 532 nm. The

dye laser is set to 469 nm (Stilbene 430 dye, Exciton, 355 nm excitation) for $S_1 \leftarrow S_0$ excitation. For $S_2 \leftarrow S_0$ excitation, 292 nm pulses are generated by Type I second harmonic generation (KDP) of 584 nm pulses (R6G dye, Eastman, 532 nm excitation). Emission is collected from the sample through a 40x reflecting microscope objective (Ealing) and sent through a polarizing cube beamsplitter (Newport) to two detection channels comprised of subtractive double monochromators (Spectral Products CM112) and microchannel plate PMT detectors (Hamamatsu R3809U-50). The reference channel is a photodiode (Becker & Hickl PHD-400). Signals are processed using commercial TCSPC electronics (Becker & Hickl SPC-132) and acquired using software written in-house using LabVIEW® code. Data reported here are the averages and standard deviations ($\pm$ 1 σ) of at least six individual acquisitions. All measurements were performed at 293 ± 1 K.

Steady state measurements. Steady state excitation and emission spectra were acquired using s SPEX Fluorolog 3 spectrometer. For all measurements the excitation and emission monochromators were set to 1 nm resolution.

Results and Discussion

The focus of this work is on measuring the rotational diffusion dynamics of tetracene in n-alkanes (Fig. 2.1) under conditions of $S_1 \leftarrow S_0$ and $S_2 \leftarrow S_0$ excitation, and using this information to better understand the consequences of local heating.

For all measurements, emission from the S_1 state is monitored (510 nm). Tetracene in

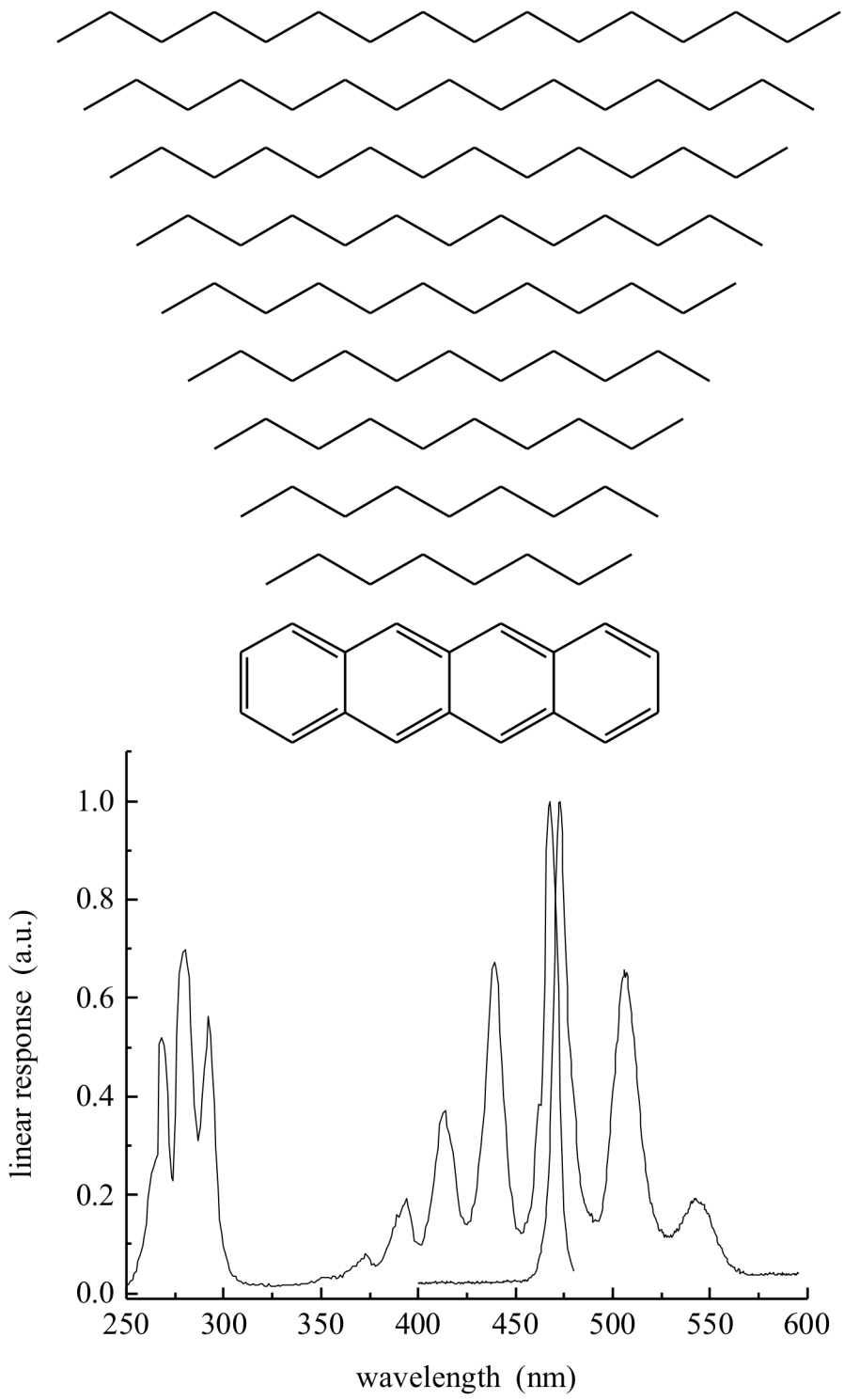

Figure 2.1 Structures of the alkanes *n*-octane through *n*-hexadecane, tetracene, and the normalized absorbance and emission spectra of tetracene in *n*-nonane. The absorbance and emission spectra of tetracene is essentially unchanged in the other *n*-alkane solvents.

solution is characterized by a fluorescence quantum yield of less than unity so some amount of

excitation energy deposited into the S_1 state decays nonradiatively, but for all measurements this is constant. According to Kasha's rule,[25] nonradiative relaxation from the S_2 to the S_1 manifold is rapid (*ca*. 1 ps). For $S_2 \leftarrow S_0$ excitation, 1.602 eV of excess energy is dissipated into the bath surrounding the chromophore during $S_1 \leftarrow S_2$ relaxation. It is this excess energy that is seen as thermal energy, dissipated primarily into the vibrational modes of the bath, initially. The result is that the immediate environment of the chromophore experiences a temperature increase, with subsequent dissipation of the energy into the solvent bath by means of intramolecular and intermolecular vibrational and rotational energy transfer. By measuring the rotational motion of the chromophore under conditions of this excess energy being present and absent, we can gauge the transient temperature increase of the chromophore local environment that results from the introduction of the excess energy.

Before we discuss the transient temperature changes experienced by these systems, we need to consider several issues. First among them is the question of whether or not the two different excitation methods ($S_1 \leftarrow S_0$ and $S_2 \leftarrow S_0$) yield information that can be compared directly. For both measurements, emission from the $S_0 \leftarrow S_1$ transition is detected. The anisotropy decay function, which contains the information of interest, is calculated from the polarized emission transients according to Eq. 1.3. The functional form of R(t) contains information about the rotational diffusion constant, D, and there is well-established body of theoretical understanding for rotational diffusion,[26-32] and the theory developed by Chuang and Eisenthal is well suited to the treatment of these data.[26] For tetracene it is known that the $S_1 \leftarrow S_0$ transition is polarized along the chromophore long in-plane axis, which we designate as *x*, and the $S_2 \leftarrow S_0$ transition is polarized along the chromophore short in-plane axis (*y*). Under these conditions, if the dominant axis of rotation for tetracene is the *x*-axis then a single exponential

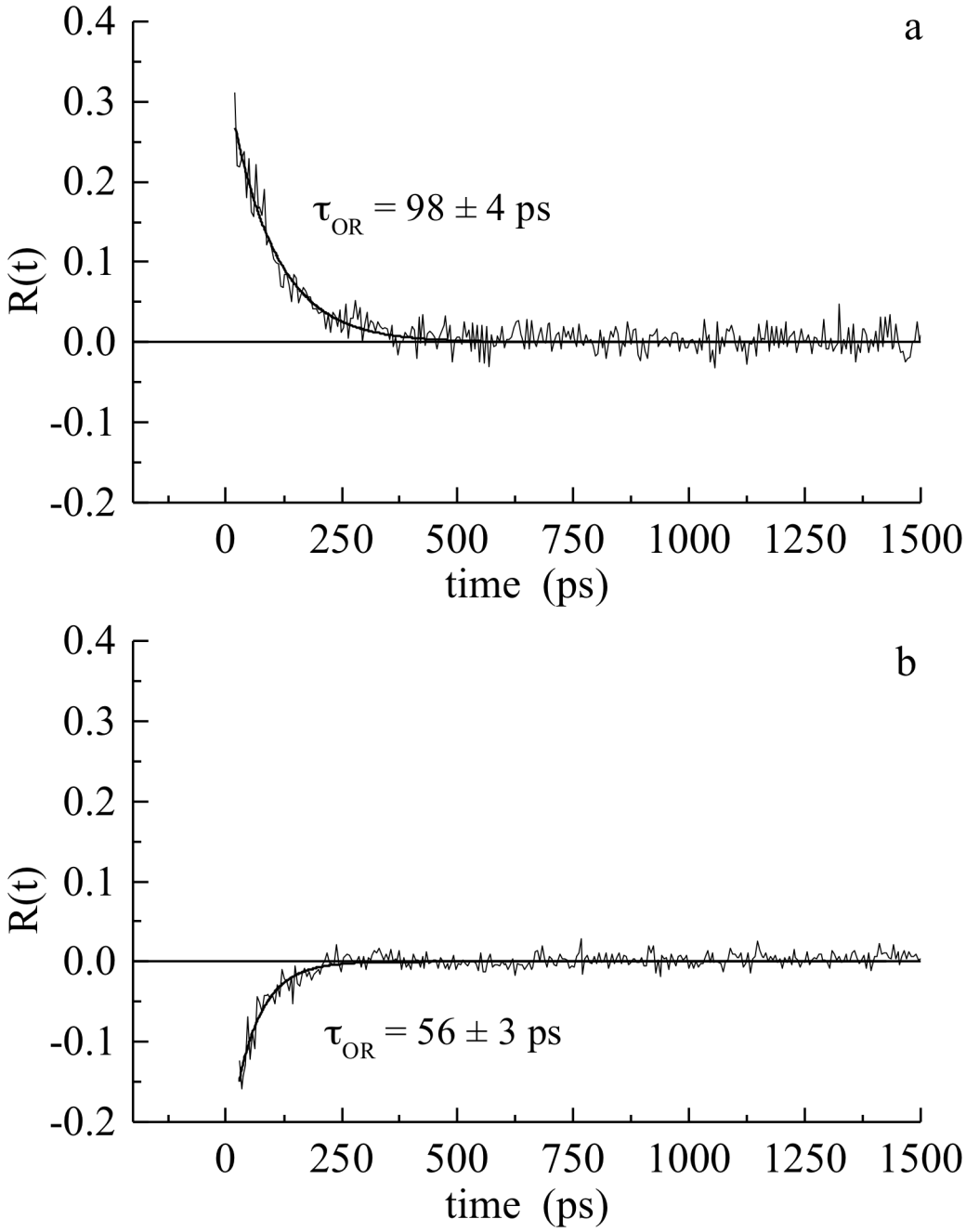

Figure 2.2 (a) Anisotropy decay data for tetracene in *n*-dodecane with $S_1 \leftarrow S_0$ excitation and $S_0 \leftarrow S_1$ emission. The solid line through the data is the best fit single exponential decay function. For this individual determination the reorientation time constant is 98 ± 4 ps. (b) Anisotropy decay data for tetracene in *n*-dodecane with $S_2 \leftarrow S_0$ excitation and $S_0 \leftarrow S_1$ emission. The solid line through the data is the best fit single exponential decay function. For this individual determination the reorientation time constant is 56 ± 3 ps.

anisotropy decay is expected, and if the dominant rotational axis is the *z*-axis a two component

decay is expected. For all of the measurements we report here we observe a single component exponential decay of R(t), consistent with tetracene rotating as a prolate rotor, with $D_x > D_y = D_z$. Given the different polarization of the $S_2 \leftarrow S_0$ transition, we must consider whether the measured anisotropy decay for both excitation conditions can be compared directly. The anisotropy decay equation for a prolate rotor with excitation and emission transitions polarized along the dominant axis of rotation is

$$R(t) = 0.4\exp(-6D_z t) \qquad [2.1]$$

And for the excitation and emission transitions polarized perpendicular to one another,

$$R(t) = -0.2\exp(-6D_z t) \qquad [2.2]$$

Thus, for both $S_1 \leftarrow S_0$ and $S_2 \leftarrow S_0$ excitation the anisotropy decay function is sensitive to the same component, D_z, of the rotational diffusion constant, D. The prediction of Eqs. 2.1 and 2.2, that the anisotropy decay function will be positive for $S_1 \leftarrow S_0$ excitation and negative for $S_2 \leftarrow S_0$ excitation is verified experimentally (Fig. 2.2).

Because the functional form of the anisotropy decay function is a single exponential it is not possible to evaluate whether or not the ratio D_z/D for tetracene changes on excitation to the S_2, but the time constants we recover from the experimental data are directly comparable. We present the reorientation time data for tetracene in the *n*-alkanes, for both S_1 and S_2 excitation, in Figure 2.3. What is immediately apparent from these data is that the reorientation time constants for S_2 excitation are smaller than the time constants for S_1 excitation for alkanes C_{10} and longer. This phenomenon has been observed previously and is known to occur as a result of transient heating in solution. We will consider the information content of this result after we examine the

dependence of the orientational relaxation time of tetracene on alkane length for the two excitation wavelengths separately.

The modified Debye-Stokes-Einstein (DSE) model (Eq. 1.7) has been used extensively in the treatment of molecular reorientation,[27-30] In this model η is the viscosity of the solvent, V is the hydrodynamic volume of the solute (209 $Å^3$ for tetracene),[33] f is a frictional factor to account for the interactions between solvent and solute,[28] k_BT is the thermal energy term and S is a shape factor to account for the non-spheroidal shape of the solute (for tetracene $S = 0.4$).[29,30] While this

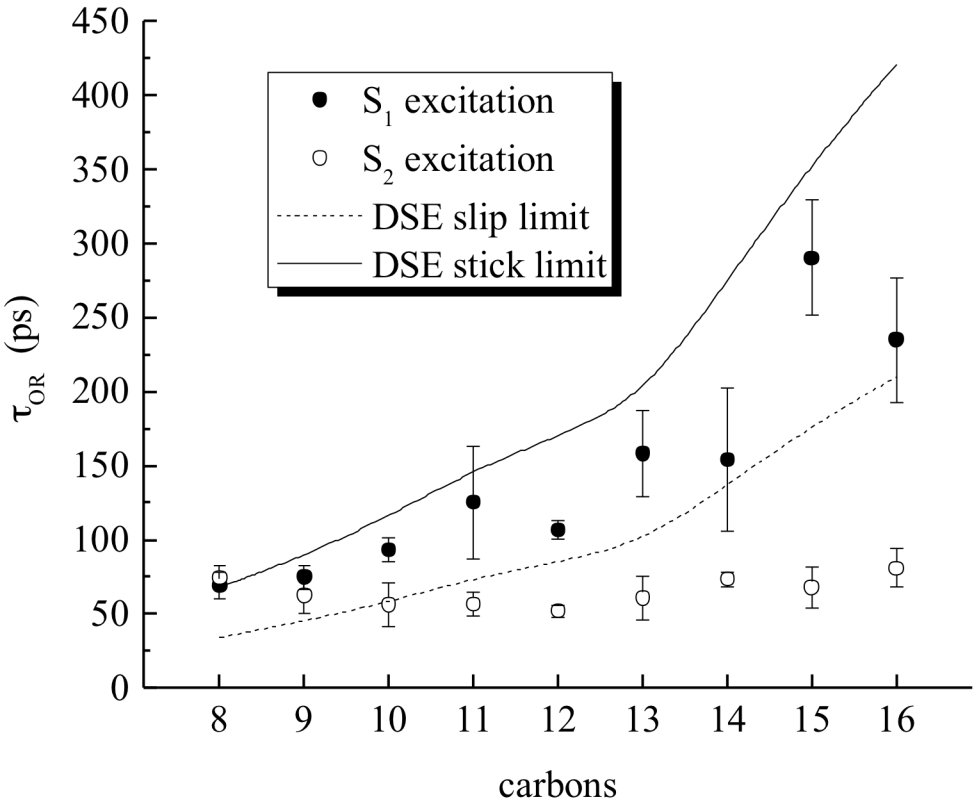

Figure 2.3 Dependence of the reorientation time constants for tetracene on the solvent alkane chain length. Data are shown for S_1 (solid circles) and S_2 (open circles) excitation, along with the predictions of the modified DSE model under stick (solid line) and slip (dotted line) limit assumptions.

model cannot account explicitly for solvent-solute molecular interactions, it has proven to be a useful model for the prediction of molecular reorientation time constants in a variety of systems. One of the more salient considerations is the value of the frictional term, *f*, for tetracene in the *n*-alkanes. In polar systems, *f* is typically taken to be 1, representative of comparatively strong frictional interactions between solvent and solute, and this is known as the "stick" limit. For non-polar systems, the "slip" limit, characterized by relatively weaker interactions, is indicated by a value of $f < 1$, with its precise value being related to the solute molecular dimensions and the dominant axis of rotation. For tetracene $f = 0.5$ in the slip limit. We can compare the experimental data to the modified DSE model based on these values of *V*, *f* and *S*.

For excitation of the $S_1 \leftarrow S_0$ transition, tetracene in *n*-alkanes exhibits reorientation that is intermediate between the stick and slip limits (Fig. 2.3). This finding, in and of itself, is not surprising. While tetracene and the *n*-alkanes are certainly non-polar species, the π-system of tetracene is polarizable. Thus interactions stronger than the slip limit but weaker than the stick limit may be expected. We note that tetracene has been reported to exhibit sub-slip behavior in several *n*-alcohols.[34] What is of greater interest, however, is the trend in the reorientation time for the longer *n*-alkanes. There emerges a clear odd-even trend in these data that depends on the number of carbons in the solvent molecules. This finding is unexpected but provides a great deal of insight into the intermolecular interactions that characterize the tetracene / *n*-alkanes systems.

For excitation of the $S_2 \leftarrow S_0$ transition of tetracene, the recovered reorientation times exhibit a fundamentally different solvent dependence. The fact that the reorientation of the chromophore is substantially different for S_2 excitation compared to S_1 excitation is indicates that excess thermal energy dissipated rapidly by tetracene upon excitation alters the local

environment of the chromophore on a timescale faster than its rotational motion. For all solvents, τ_{OR} for S_2 excitation is sub-slip and there is seen to be almost no solvent-dependence. The details of the dependence of τ_{OR} on solvent for S_2 excitation is unexpected, and while it may be tempting to draw larger conclusions from this nominal solvent-independence, we refrain from doing so at this point, in favor of using this information to evaluate the transient temperature change experienced by the solvent in closest proximity to the chromophore.

The difference in tetracene τ_{OR} for S_1 and S_2 excitation in each alkane reflects the transient temperature change experienced by the chromophore as a result of dissipating *ca*. 1.6 eV of energy nonradiatively. We recognize that the temperature of the chromophore local environment is changing on the timescale of molecular rotation and, as such, we cannot obtain quantitative information on the maximum ΔT or on the functional form of the dissipation of the thermal energy in these systems. Despite these limitations we can estimate ΔT as a function of solvent using a treatment we have detailed previously.[22-24]

The ability to infer the transient temperature change from state-dependent reorientation data is based on the temperature dependence of the solvent viscosity,[22]

$$\Delta\tau_{OR} = \tau_{OR}^{S_2} - \tau_{OR}^{S_1} = \Delta\left(\frac{\eta}{T}\right)\frac{Vf}{k_B S} \qquad [2.3]$$

For the *n*-alkanes the temperature dependence of their bulk viscosity is well characterized[35] and the experimentally determined $\Delta\tau_{OR}$ can be used to infer $\Delta\eta$. We note that extracting temperature-change information from our experimental data using this model requires some assumptions to be made. Specifically, it is also possible, in principle, for the frictional interaction factor, *f*, in Eqs. 2.2 and 2.3 to exhibit a temperature-dependence. We assert that the

rigid structure of the probe renders the shape factor, S, largely independent of temperature. In the interpretation that follows we have made the assumption that f is nominally the same for *a given solvent* for both excitation conditions because the fundamental nature of the physical interactions between tetracene and the solvent molecules surrounding it remain the same.

With these limitations in mind, we estimate ΔT using Eq. 5. From $\Delta\eta$ and known values for η and a function of T, ΔT can be calculated directly. We present these data in Table 2.1 and Fig. 2.4.

Solvent	**η (cP)**	**$\tau_{OR}{}^{S}{}_{1}$ (ps)**	**$\tau_{OR}{}^{S}{}_{2}$ (ps)**	**$\Delta\tau_{OR}$ (ps)**	**$\Delta\eta$ (cP)**	**ΔT (K)**
C_8	0.54	69 ± 9	75 ± 8	6 ± 17	0.04 ± 0.14	0 ± 13
C_9	0.71	75 ± 8	62 ± 12	-13 ± 20	-0.10 ± 0.16	13 ± 25
C_{10}	0.92	93 ± 8	56 ± 15	-37 ± 23	-0.29 ± 0.19	29 ± 26
C_{11}	1.17	125 ± 38	56 ± 8	-69 ± 46	-0.55 ± 0.36	46 ± 33
C_{12}	1.35	107 ± 6	52 ± 4	-55 ± 10	-0.44 ± 0.08	27 ± 7
C_{13}	1.55	158 ± 29	60 ± 15	-98 ± 44	-0.78 ± 0.35	48 ± 27
C_{14}	2.18	154 ± 48	73 ± 5	-81 ± 53	-0.64 ± 0.42	20 ± 17
C_{15}	2.81	290 ± 39	68 ± 14	-222 ± 53	-1.76 ± 0.42	60 ± 25
C_{16}	3.34	235 ± 42	81 ± 13	-154 ± 55	-1.22 ± 0.44	18 ± 11

Table 2.1 Reorientation time constants, viscosity and temperature change as a function of solvent alkane chain length

These data contain several interesting features. The first is that the magnitude of the changes in temperature associated with the dissipation of 1.6 eV of excess energy are somewhat higher than have been reported previously for different chromophores (Rhodamine 640 and

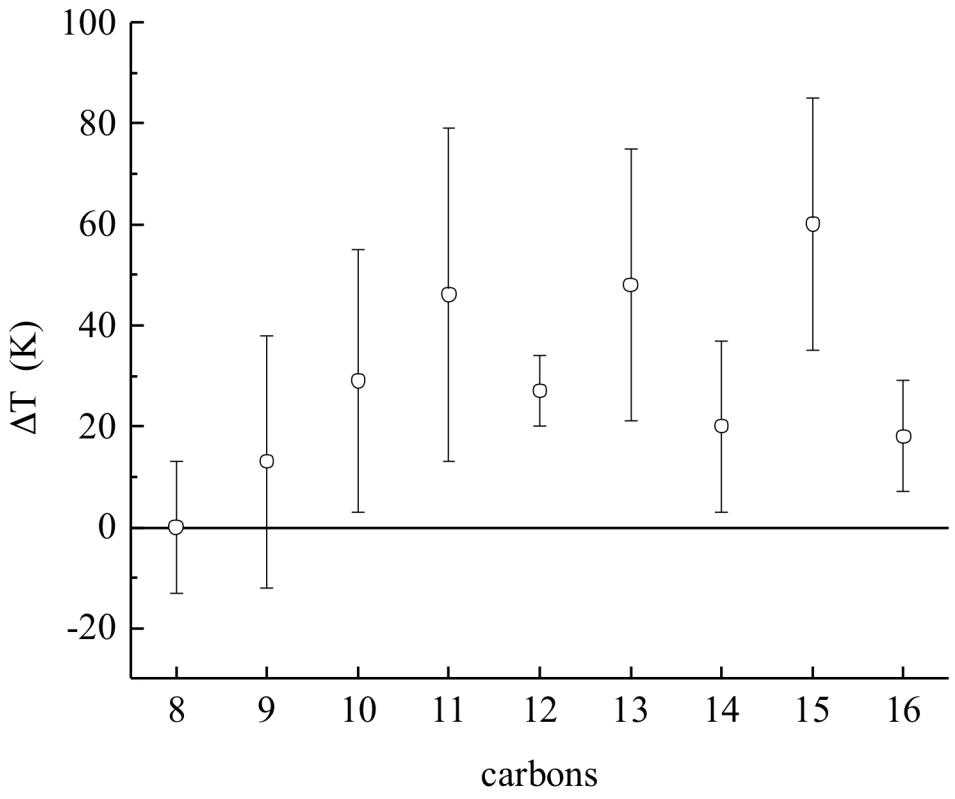

Figure 2.4 Calculated transient temperature change associated with the dissipation of excess energy as a function of solvent alkane chain length.

perylene) in both polar bulk solvent[22] and lipid bilayer environments.[23,24] In those bodies of work the transient temperature changes were somewhat smaller, on the order of 10 K. In this work we observe significantly larger temperature changes. We understand this finding for bulk liquids in the context of the nature of solvent-solvent interactions for polar and non-polar solvents. For polar protic solvents, hydrogen-bonding and dipole-dipole interactions give rise to strong coupling between solvent molecules. For non-polar systems, van der Waals interactions dominate, and these interactions are shorter range in nature. For this reason we expect solvent-solvent coupling for non-polar solvents to be substantially weaker than it is for polar systems, and this expectation is borne out by comparing the thermal conductivity of *n*-alkanes and *n*-alcohols.[37]

It is also important to consider that the temperature change sensed by the reorientation measurements is averaged over the reorientation time constant, so that shorter reorientation times will yield observed transient temperature changes that are larger than longer reorientation times, assuming the thermal energy relaxation time is always faster than the chromophore reorientation time. For the *n*-alcohols studied using a polar chromophore, the reorientation times ($S_1 \leftarrow S_0$ excitation) were in the range of 134 ps to 3439 ps, resulting in temperature changes on the order of 10 K or less.[22] In this work, the range of reorientation times ($S_1 \leftarrow S_0$ excitation) are 69 to 290 ps, with commensurately larger temperature changes being inferred from these data. The results we report here for *n*-alkanes are thus not surprising.

We have investigated transient temperature change effects for perylene, a non-polar chromophore localized in the acyl chain region of phospholipid bilayers.[23,24] In that work the anisotropy decay functionality was biexponential, with the longest time constant being on the order of 2500 ps. The transient temperature changes found in that work were dependent on the extent of lipid acyl chain organization and were on the order of 10 K. While those temperature changes appear to be much smaller than those reported here, we believe that there is no inconsistency. In addition to the difference in the time resolution used to sense the temperature change, the presence of an aqueous layer in close proximity to the lipid bilayer structures suggests more efficient energy transfer than is seen in *n*-alkane liquids. The transient temperature change data we report here are consistent with expectations.

Of particular significance is the odd-even effect that we observe, both in the reorientation data for $S_1 \leftarrow S_0$ excitation and in the transient temperature change data. Since the transient temperature change data are derived from the reorientation data, the fact that we observe the

same effect in both cases is not surprising. The perspectives offered by the two different manifestations of this effect do, however, provide some useful insight into the phenomena that are likely responsible for its prominence. There is long history of observing odd-even effects in *n*-alkanes,[38] with recent work being focused on low temperature x-ray diffraction data taken on crystalline *n*-alkanes.[39] The origin of odd-even effects in *n*-alkanes is thought to be related to the symmetry of the all-trans *n*-alkanes. Even *n*-alkanes possess a center of inversion whereas odd *n*-alkanes do not. A consequence of this is that the unit cell of even *n*-alkanes is one molecule in size and for odd *n*-alkanes it is two molecules in size, resulting in a slight density difference in the two cases owing to the ability of the *n*-alkanes to pack. The orientations of the terminal methyl groups is the key structural issue. As noted in that work, such a subtle change in crystal structure indicates a small odd-even modulation in density, and this is not seen experimentally, especially in room temperature liquids. The observation of a pronounced odd-even solvent effect in room temperature liquid alkanes is surprising.

It is well established that room temperature liquid *n*-alkanes do not exist predominantly in their all-trans conformation.[40-43] The majority of *n*-alkane molecules are characterized by one or more gauche conformers, with the fraction of gauche bonds depending on the length of the *n*-alkane and the temperature of the system. We have studied the ground state vibrational relaxation behavior of tetracene in *n*-alkanes previously and in that work we found evidence for comparatively efficient transfer of vibrational energy between several tetracene S_0 ring distortion modes (in the 1200 cm^{-1} to 1500 cm^{-1}) range and the alkane bath acceptor modes, including the 1375 cm^{-1} terminal methyl group rocking mode.[10] Because of the aspect ratio of the tetracene molecule and the dependence of the measured T_1 times on solvent chain length, we postulated that tetracene may have a templating effect on the solvent in its immediate proximity. Due to

favorable intermolecular interactions for alkane all-trans conformers with tetracene,[44,45] the chemical structure of the solute can produce a local enhancement in the fraction of solvent molecules that are in a predominantly all-trans conformation. That assertion is consistent with the reorientation data we present here, where an odd-even effect is seen only for alkanes that are longer than the tetracene molecule (*i.e.* C_{11} and higher). If, in fact this templating effect is occurring, it would be consistent with the transient temperature change data we elucidated in this work. By analogy to the low temperature x-ray measurements, if the tetracene chromophore is templating the solvent to be in a predominantly trans conformation, the average distance between the chromophore and solvent terminal methyl groups will be slightly larger for the odd alkanes than it is for the even alkanes. In this model, the higher transient temperature changes seen for the odd alkanes is correlated with a greater distance and/or orientational mismatch, on average, between the tetracene ring system (vibrational donor) and the alkane solvent terminal methyl groups (vibrational acceptors). If this correlation is relevant to the phenomenon we observe, a clear implication would be that the tetracene ring breathing and distortion modes are gateway donor modes for the intermolecular transfer of (vibrational) energy from tetracene to the terminal methyl group rocking modes of the bath. Owing to the persistence time of the observed heating effect, it appears that the nature of intermolecular energy transfer between alkanes that occurs subsequent to the initial energy transfer from tetracene to the bath must also proceed in a solvent-dependent manner. Subtle differences between odd and even length alkanes must be responsible for the observed effect and this finding implies a level of solvent organization that is not typically characteristic of liquid alkanes. Such a condition is consistent with tetracene having an influence on the organization of the solvent molecules in closest proximity.

Conclusions

We have measured the rotational diffusion time constants of tetracene in *n*-alkanes C_8 through C_{16}, and for excitation of the tetracene S_1 and S_2 states. Our data demonstrate several interesting features. The first is that for S_2 excitation of tetracene, the reorientation time is seen to be almost independent of solvent aliphatic chain length. This is due to transient heating associated with the radiationless dissipation of *ca*. 1.6 eV of excess energy during rapid relaxation from the tetracene S_2 state to the S_1 state. The transient heating effect is expected and is especially pronounced in this system because of the characteristically fast dynamics of tetracene in alkanes and the modest thermal conductivity of the alkane solvents. The second interesting feature of these data is that for excitation of the S_1 state of tetracene, solvent-dependent reorientation is seen that exhibits an odd-even effect. This is likely associated with the relative proximity of the chromophore and the solvent terminal methyl groups. Based on our experimental data, it appears the chromophore itself is exerting an influence on the *n*-alkane solvent molecules in closest proximity, which accounts for the pronounced odd-even effects we observe. The fact that analogous odd-even effects are not seen for other polycyclic aromatic hydrocarbon chromophores in the same alkane solvents[6-8] argues for the shape of the chromophore having a templating effect on the surrounding solvent.

REFERENCES

REFERENCES

1. Assael, M. J.; Dymond, J. H.; Papadaki, M.; Patterson, P. M., Correlation and prediction of dense fluid transport coefficients. I. *n*-Alkanes. *International Journal of Thermophysics* **1992**, *13*, 269-281.

2. Assael, M. J.; Dymond, J. H.; Tselekidou, V., Correlation of high pressure thermal conductivity, viscosity and diffusion coefficients for n-alkanes. *International Journal of Thermophysics* **1990**, *11*, 863-873.

3. Watanabe, H.; Seong, D. J., The thermal conductivity and thermal diffusivity of liquid *n*-alkanes: C_nH_{2n+2} (n=5 to 10) and toluene. *International Journal of Thermophysics* **2002**, *23*, 337-356.

4. Goldie, S. N.; Blanchard, G. J., Orientational and Vibrational Relaxation Dynamics of Perylene and 1-Methylperylene in n-Alcohols: Probing the Balance between van der Waals and Hydrogen-Bonding Interactions. *J. Phys. Chem. A* **1999**, *103*, 999-1006.

5. Goldie, S. N.; Blanchard, G. J., Orientational and Vibrational Relaxation Dynamics of Perylene and 1-Methylperylene in Aldehydes and Ketones. *J. Phys. Chem. A* **2001**, *105*, 6785-6793.

6. Jiang, Y.; Blanchard, G. J., Vibrational Population Relaxation of Perylene in n-Alkanes. The Role of Solvent Local Structure in Long-Range Vibrational Energy Transfer. *J. Phys. Chem.* **1994**, *98*, 9411-9416.

7. Jiang, Y.; Blanchard, G. J., Vibrational Population Relaxation of Perylene in Its Ground and Excited Electronic States. *J. Phys. Chem.* **1994**, *98*, 9417-9421.

8. Jiang, Y.; Blanchard, G. J., Vibrational Population and Orientational Relaxation Dynamics of 1-Methylperylene in n-Alkanes. The Effective Range of Dipolar Energy Relaxation in Solution. *J. Phys. Chem.* **1995**, *99*, 7904-7912.

9. Jiang, Y.; McCarthy, P. K.; Blanchard, G. J., The role of multiple electronic states in the dissipative energy dynamics of Coumarin 153. *Chem. Phys.* **1994**, *183*, 249-267.

10. McCarthy, P. K.; Blanchard, G. J., Vibrational Population Relaxation of Tetracene in n-Alkanes. Evidence for Short-Range Molecular Alignment. *J. Phys. Chem.* **1995**, *99*, 17748-17753.

11. McCarthy, P. K.; Blanchard, G. J., Solvent Methyl Group Density Dependence of Vibrational Population Relaxation in 1-Methylperylene: Evidence for Short-Range Organization in Branched Alkanes. *J. Phys. Chem.* **1996**, *100*, 5182-5187.

12. Elsaesser, T.; Kaiser, W., Vibrational and vibronic relaxation of large polyatomic molecules in liquids. *Annual Review of Physical Chemistry* **1991**, *42*, 83-107.

13. Lingle, R. J.; Xu, X.; Yu, S.-C.; Zhu, H.; Hopkins, J. B., Ultrafast investigation of condensed phase chemical reaction dynamics using transient vibrational spectroscopy: Geminate recombination, vibrational energy relaxation, and electronic decay of the iodine A' excited state. *J. Chem. Phys.* **1990**, *93*, 5667-6580.

14. Heilweil, E. J.; Casassa, M. P.; Cavanagh, R. R.; Stephenson, J. C., Population lifetimes of OH(v=1) and OD(v=1) stretching vibrations of alcohols and silanols in dilute solution. *J. Chem. Phys.* **1986**, *85*, 5004-5018.

15. Hill, J. R.; Dlott, D. D., A model for ultrafast vibrational cooling in molecular crystals. *J. Chem. Phys.* **1988**, *89*, 830-841.

16. Hill, J. R.; Dlott, D. D., Theory of vibrational cooling in molecular crystals: Application to crystalline naphthalene. *J. Chem. Phys.* **1988**, *89*, 842-858.

17. Chang, T.-C.; Dlott, D. D., Vibrational cooling in large molecular systems: Pentacene in naphthalene. *J. Chem. Phys.* **1989**, *90*, 3590-3602.

18. Kim, H.; Dlott, D. D., Molecular dynamics simulation of nanoscale thermal conduction and vibrational cooling in a crystalline naphthalene cluster. *J. Chem. Phys.* **1991**, *94*, 8203-8209.

19. Anfinrud, P. A.; Han, C.; Lian, T.; Hochstrasser, R. M., Evolution of the transient vibrational spectrum following short pulse excitation. *Journal of Physical Chemistry* **1990**, *94*, 1180-1184.

20. Heilweil, E. J.; Casassa, M. P.; Cavanagh, R. R.; Stephenson, J. C., Picosecond vibrational energy transfer studies of surface adsorbates. *Annual Review of Physical Chemistry* **1989**, *40*, 143-171.

21. Heilweil, E. J.; Cavanagh, R. R.; Stephenson, J. C., Population relaxation of CO(v=1) vibrations in solution phase metal carbonyl complexes. *Chemical Physics Letters* **1987**, *134*, 181-188.

22. Dela Cruz, J. L.; Blanchard, G. J., Reorientation Dynamics of Rhodamine 640 in Normal Alcohols: Measurement of the Length and Time Scale of Transient Local Heating in Solution. *J. Phys. Chem. A* **2001**, *105*, 9328-9335.

23. Pillman, H. A.; Blanchard, G. J., The effects of energy dissipation on motional dynamics in unilamellar vesicles. *Journal of Physical Chemistry B* **2010**, *114*, 13073-13079.

24. Pillman, H. A.; Blanchard, G. J., Consequences of transient heating on the motional dynamics of cholesterol-containing phospholipid vesicles. *Journal of Physical Chemistry B* **2011**, *115*, 3819-3827.

25. Kasha, M., Characterization of electronic transitions in complex molecules. *Discussions of the Faraday Society* **1950**, *9*, 14-19.

26. Chuang, T. J.; Eisenthal, K. B., Theory of fluorescence depolarization by anisotropic rotational diffusion. *J. Chem. Phys.* **1972**, *57*, 5094-5097.

27. Debye, P. *Polar Molecules* Chemical Catalog Co.: New York 1929.

28. Hu, C.-M.; Zwanzig, R., Rotational friction coefficients for spheroids with the slipping boundary condition. *J. Chem. Phys.* **1974**, *60*, 4354-4357.

29. Perrin, F., Mouvement brownien d'un ellipsoide (I). Dispersion dielectrique pour les molecules ellipsoidale. *Le Journal de Physique et le Radium* **1934**, *5*, 497.

30. Perrin, F., Mouvement Brownien d'un ellipsoide (II). Rotation libre et depolarisation des fluorescences. Translation et diffusion de molecules ellipsoidales. *Le Journal de Physique et le Radium* **1936** *7*, 1-11.

31. Favro, D. L., Theory of the Rotational Brownian Motion of a Free Rigid Body. *Physical Review* **1960**, *119*, 53-62.

32. Tao, T., Time-Dependent Fluorescence Depolarization and Brownian Rotational Diffusion Coefficients of Macromolecules. *Biopolymers* **1969**, *8*, 609-632.

33. Edward, J. T., Molecular volumes and the Stokes-Einstein equation. *Journal of Chemical Education* **1970**, *47*, 261-270.

34. Wirth, M. J.; Chou, S.-H., Behavior of the rotational diffusion tensor of tetracene under sub-slip conditions. *Journal of Physical Chemistry* **1991**, *95*, 1786-1789.

35. *CRC Handbook of Chemistry and Physics*; Lide, D. R., Ed.; CRC Press, Inc.: Boca Raton, FL, 1990-1991; Vol. 71.

36. Gray, C. G.; Gubbins, K. E. *Theory of Molecular Fluids, Vol. 1: Fundamentals*; Oxford Science: Oxford, UK, 1984.

37. Kauffman, G. W.; Jurs, P. C., Prediction of surface tension, viscosity, and thermal conductivity for common organic solvents using quantitative structure-property relationships. *Journal of Chemical Information and Computational Science* **2001**, *41*, 408-418.

38. Baeyer, A., Ueber Regelmassigkeiten im Schmekspunkt Homologer Verbindungen. *Berichte der deutschen chemischen Geselshaft* **1877**, *10*, 1286-1288.

39. Boese, R.; Weiss, H.-C.; Blaser, D., The melting point alternation in the short chain *n*-alkanes: Single-crystal X-ray analyses of propane at 30 K and *n*-butane to *n*-nonane at 90 K. *Angewandte Chemie Int. Ed.* **1999**, *38*, 988-992.

40. Ryckaert, J.-P.; Bellemans, A., Molecular dynamics of liquid alkanes. *Faraday Discussions of the Chemical Society* **1978**, *66*, 95-106.

41. Almarza, N. G.; Enciso, E.; Alonso, J.; Bermejo, F. J.; Alvarez, M., Monte Carlo Simulations of liquid n-butane. *Molecular Physics* **1990**, *70*, 485-504.

42. Fischer, E. W.; Strobl, G. R.; Dettenmaier, M.; Stamm, M.; Steidle, N., Molecular orientational correlations and local order in n-alkane liquids. *Faraday Discussions of the Chemical Society* **1979**, *68*, 26-45.

43. Schoen, P. E.; Priest, R. G.; Sheridan, J. P.; Schnur, J. M., Pressure induced changes in liquid alkane chain conformation. *J. Chem. Phys.* **1979**, *71*, 317-323.

44. Wallenborn, E.-U.; Wild, U. P., Analysis of the optical spectra of aromatic-alkane clusters. *J. Chem. Phys.* **1997**, *107*, 8338-8348.

45. Ben-Horin, N.; Even, U.; Jortner, J., Microscopic and macroscopic solvation of aromatic molecules in aliphatic hydrocarbons. *Chemical Physics Letters* **1991**, *177*, 153-160.

CHAPTER 3

Interface-mediation of lipid bilayer organization and dynamics

This chapter is adapted from Hannah E. Mize and G. J. Blanchard, "Interface-Mediation of Lipid Bilayer Organization and Dynamics," Physical Chemistry Chemical Physics (PCCP), **18**, 16977-16985 (2016).

Introduction

Chemical sensing requires two distinct functions; molecular selectivity and signal transduction. Achieving chemical selectivity is a substantial challenge that has been achieved successfully by living biological systems, and the transduction of a chemical signal into one that is quantifiable (*e.g.* photons or electrons) is comparatively well established.[1,2] The components that perform these two functions are connected directly, with the transducer typically functioning as the support or mount for the chemically selective component.

The use of biomolecules as selective entities is appealing based on the known chemical selectivity of transmembrane proteins and enzymes. The ability of transmembrane proteins to function is mediated by the composition and morphology of the plasma membrane surrounding them, for reasons of protein folding and mobility, and the replication of such a system in the laboratory is not a simple task. The mammalian plasma membrane is known to contain in excess of 500 unique molecular constituents,[3] and there is a limited amount of detailed information available on the fluidity or spatial heterogeneity of the plasma membrane. One approach to developing biosensors that use transmembrane proteins is to design synthetic bilayers containing a limited number of components,[4,5] but a significant limitation to this approach lies in the ill-understood relationship between bilayer composition and protein folding. We have undertaken a series of studies of model bilayer structures with an eye toward understanding the relationship between composition and environmental factors, and the observed phase segregated organization

of these systems.[6-18] In this work we focus on model lipid bilayer structures covered by an aqueous overlayer and supported on a planar mica surface.

In this structural format, supported lipid bilayers exhibit phase segregation, with cholesterol-rich regions separating from phosphocholine-rich regions. The characteristic sizes and shapes of these cholesterol-rich domains are determined by the minimization of the sum of interfacial energies within the system. For a simple two-component system one would expect a single phase boundary, however this is not the case for supported bilayers. The lowest energy structure is determined from the energies of interaction between the support and the aqueous overlayer, with each bilayer phase and the phase boundaries in the bilayer plane.[19,20] We can thus exert some control over the domain size of the cholesterol-rich regions of our supported bilayers through changes in the composition of the aqueous overlayer (*e.g.* ionic strength and pH).

Controlling model bilayer phase segregation is an important first step in establishing control over the folding of transmembrane proteins, but it is not clear from data showing mesoscopic phase segregation how the fluidity and local dynamics of the bilayer constituents are influenced by changes in the bilayer morphology. Consequently, we incorporate a small amount (*ca*. 1 mol%) of a tethered fluorescent probe into these bilayer structures and monitor rotational diffusion dynamics to gauge how the local environment of the chromophore is affected by variations in the aqueous overlayer pH and ionic strength. A rhodamine derivative that is bound covalently to the headgroup of phosphoethanolamine is used as the chromophore. The tethered chromophore exhibits dynamics that can be modeled in the context of a hindered rotor, a well understood model.[21,22] Our data point to the dynamics of the rhodamine chromophore sensing two distinct environments within the supported bilayer, which depend differently on the pH and

ionic strength of the aqueous overlayer. The sub-population of the tethered chromophore that exhibits pH and ionic strength dependencies appears to reside in an environment characterized by stronger interactions with the chromophore compared to the sub-population in a pH and ionic strength-independent environment. We consider the chemical basis for this behavior.

Experimental Methods

Chemicals. 1,2-Dioleoyl-sn-phosphatidylcholine (DOPC), cholesterol (ovine wool), sphingomyelin (chicken egg) and sulforhodamine tagged 1,2-dioleyol-*sn*-phospatidyl-ethanolamine (SR-DOPE), dissolved in chloroform were purchased from Avanti Polar Lipids and used as received. Trizma® Tris buffer (Sigma Aldrich), NaOH (Spectrum, Pellets, Reagent, ACS), $CaCl_2$ (Purified Grade, Anhydrous), HCl (ACS/Electronic Grade), NaCl (ACS Grade, Crystals), were purchased from CCI and used without further purification. High-grade muscovite mica used as the support was purchased from Ted Pella, Inc.

Fluorescence Anisotropy Decay Imaging (FADI). An instrument based on an inverted microscope (Nikon Eclipse Ti-U) is used to obtain fluorescence anisotropy decay images of the planar bilayers.[11,12] Detection of time-resolved data is achieved with a polarized dual channel confocal scanning instrument (Becker & Hickl DCS-120) attached to a microscope port and controlled by a galvo-drive unit (Becker & Hickl GDA-120). The confocal scanner is equipped with a polarizing beam splitter and two avalanche photodiode detectors (ID-Quantique ID100) for the acquisition of fluorescence lifetime and anisotropy decay images. Polarized fluorescence transients used in the generation of fluorescence lifetime and anisotropy images are acquired using time-correlated single photon counting detection electronics (Becker & Hickl SPC-152, PHD-400N reference diode). The time-correlated single photon counting (TCSPC) and confocal

scanning instruments are controlled by commercial software (Becker & Hickl) run on a windows-based PC.

The light source for this instrument is a synchronously pumped, cavity-dumped dye laser (Coherent 702-2) excited using a passively-mode locked Nd:YVO_4 laser (Spectra Physics Vanguard). The output of the excitation laser is a train of 13 ps pulses at a repetition rate of 80 MHz. The second harmonic and third harmonic outputs of this laser (532 nm, 355 nm) are used to pump the dye lasers. In this work the dye laser was excited with the second harmonic output (2.5 W average power) and Pyrromethene 567 (Exciton) was used as the laser dye. The dye laser repetition rate, determined by the cavity dumping electronics, is 4 MHz (250 ns between pulses), with 5 ps pulses at 563 nm.

Time-Resolved Fluorescence Measurements. The system used to acquire anisotropy decay data on vesicles suspended in solution has been described elsewhere and we provide only a brief overview here.[23] The light source used for this instrument is identical to that used for the TCSPC imaging measurements (vide supra). Emission collection was accomplished using a 40× reflecting microscope objective (Ealing). Emission polarization was selected using a polarizing cube beamsplitter (Newport) with separate detection channels for vertical and horizontal polarizations. Spectral selection was performed using subtractive double monochromators (Spectral Products CM112) equipped with microchannel plate PMT detectors (Hamamatsu R3809U-50). A photodiode (Becker & Hickl PHD-400) was the reference channel detector. Commercial TCSPC electronics (Becker & Hickl SPC-132) were used to process the detector signals, and the data was acquired using software written using LabVIEW®. Data processing is the same as described previously.[23]

Bilayer Preparation. The vesicles used in these experiments were formed from a mixture of the constituent species; 49 mol% DOPC, 40 mol% sphingomyelin, 10 mol% cholesterol, and 1 mol% SR-DOPE. After the chloroform was removed by evaporation, Milli-Q H_2O was added to make the overall lipid concentration 1 mg/mL. The vial was placed in a 50 °C water bath for 30 minutes, vortexed for 2 minutes, and sonicated for 30 minutes at 50 °C.[24] The resulting vesicles were deposited onto mica, and Trizma® buffer solution (10 mM, pH 7.5,100 mM NaCl) and $CaCl_2$ (2 mM aqueous solution) were added. After ten minutes of exposure time the bilayers formed by vesicle fusion were rinsed with the intended aqueous overlayer: pH between 4 and 10 at ionic strength I = 0.05, or ionic strength in the range of 0.05 to 0.4 at pH 7. Suspended vesicles used for the TCSPC measurements are the same as those used for deposition of the planar supported bilayers. The vesicles are suspended in solutions with the same ranges of pH and ionic strength as the planar bilayers.

FADI Data Collection. For each pH and ionic strength studied, a total of 3 planar bilayers were prepared. Two measurements were performed on each sample, for a total of 6 measurements. A 40x objective was used data collection. For this optical configuration the depth of focus is on the order of 1 μm. The depth resolution of the measurement is limited by the thickness of the bilayer, which is *ca*. 6 nm for the bilayers studied here. In-plane resolution of the acquired image is 256 x 256 pixels, with the physical dimension subtended by each pixel being determined by the objective used. For the 40x objective, each pixel corresponded to a 2.5 μm diameter area on the sample, *ca*. ten times the diffraction limit. For each pixel, two TCSPC channels of data are acquired, one for vertical polarization and one for horizontal polarization. Each channel has 256 time resolution elements. For a time window of 10 ns, data points were separated by 39 ps. A frame scan was used to produce an image of a defined area. These

measurements used 60 second frame acquisition times and 30 frames were collected.

Data Analysis. Fluorescence lifetime and anisotropy decay images were obtained and processed using commercial software (Optispec, Becker & Hickl). The anisotropy decay data and images were prepared using SpcImage software (Becker & Hickl). From each of the six measurements, three 25x25 pixel squares of data were extracted, for a total of 18 sets of data for each pH and ionic strength. Transients of a given polarization in the extracted region were summed and used to create the induced orientational anisotropy function, R(t). Regression of the anisotropy decay data was performed using Microcal Origin® v 9.0.

Results and Discussion

The morphological changes in supported bilayers that occur with changes in overlayer pH and ionic strength are expected based on the minimization of the overall free energy of the system.[4,5] While the thermodynamic treatment of bilayers provides the fundamental energetic basis for phase segregation, such information does not generally provide molecular-scale insight into the structural properties system, including intermolecular interactions that ultimately determine the details of system organization. Relating changes in the observed dynamics on molecular length scales to macroscopic system morphology remains to be achieved, and the data presented here will hopefully provide some useful information for making that connection.

We are concerned in the long-term with how changes in the aqueous overlayer of the lipid bilayer give rise to observed changes in the morphology and dynamics of the phase-segregated, cholesterol-rich regions of the supported bilayer structures. These phase-segregated regions are seen only when sphingomyelin is present in the bilayer.[5,11,12] It is possible, however, that phase-segregated cholesterol-rich regions are present in the absence of sphingomyelin but their characteristic domain size is smaller than can be resolved by optical microscopy (*ca*. 250

nm). This is an issue we intend to address in future work by comparing rotational and translational diffusion data in these systems.

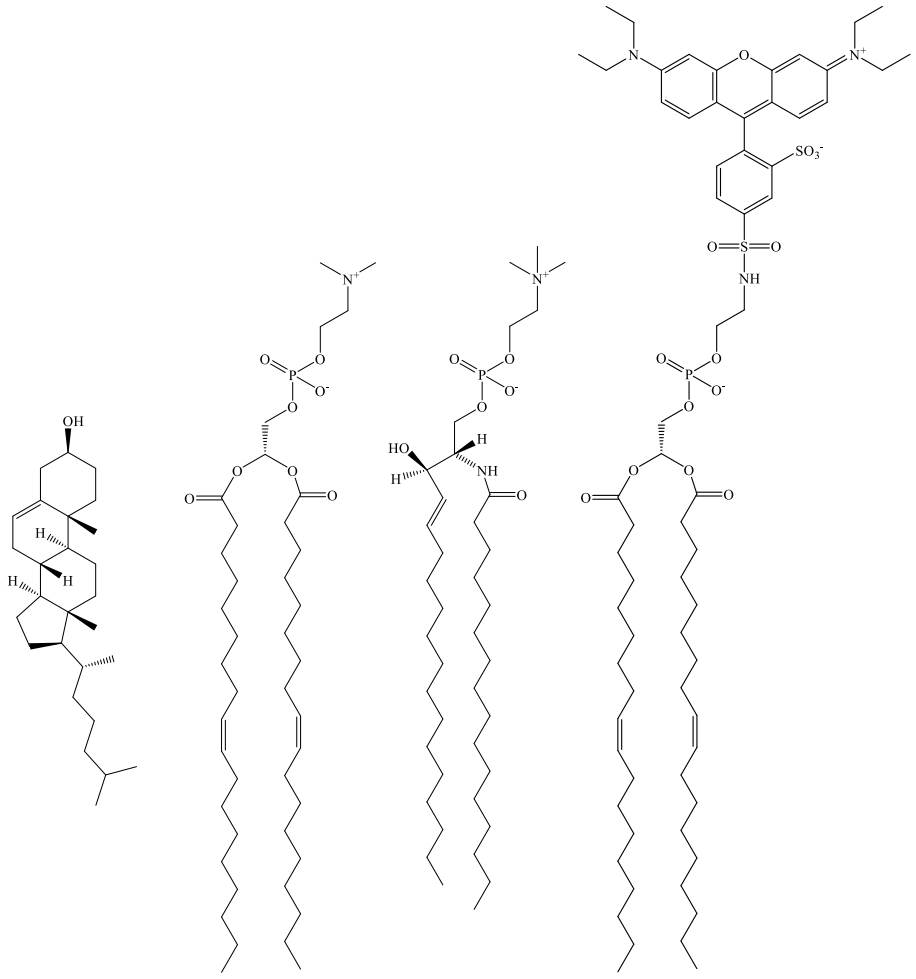

Figure 3.1 Structures of the bilayer constituents used in this work. From left to right: Cholesterol, DOPC, sphingomyelin, SR-DOPE.

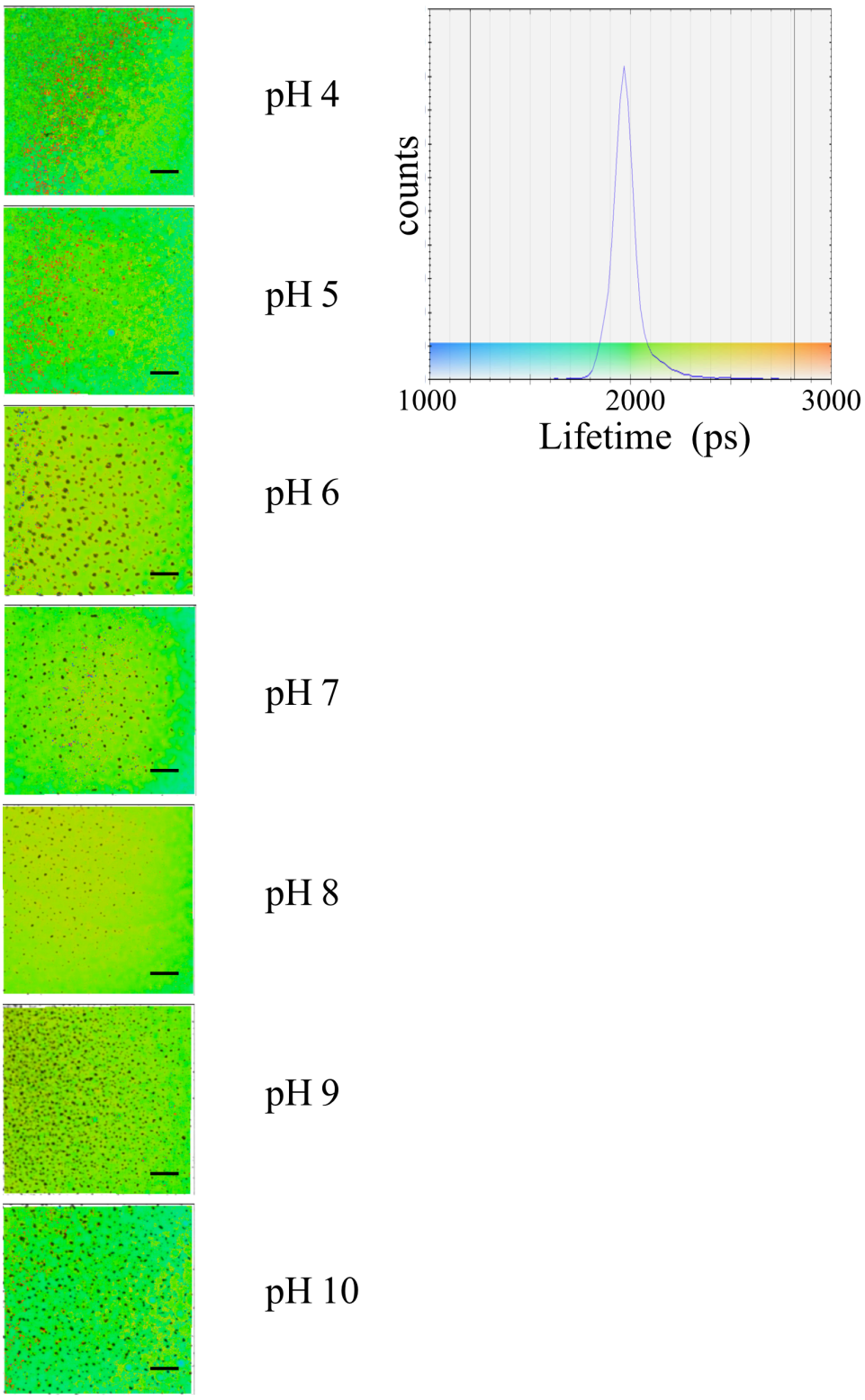

Figure 3.2 Fluorescence lifetime images for planar supported bilayers over the pH range of 4 to 10, as indicated. The scale bar in each image is 10 μm

In this work we focus on understanding the rotational diffusion dynamics of a headgroup-tethered chromophore present in a supported lipid bilayer (Fig. 3.1) under conditions where the aqueous overlayer pH and ionic strength are varied in a systematic manner. It is seen that the morphology of these systems depends on these overlayer properties (Fig. 3.2). For these measurements, the motion of the tethered rhodamine is treated in the context of the hindered rotor model by virtue of its structure and manner of incorporation into the bilayer.[21,22,25-29] In this model, the chromophore is considered to move with a restricted conic volume, and while executing this precessional motion it "wobbles" about its tethering bond. We collect polarized emission transients $I_{\|}(t)$ and $I_{\perp}(t)$ and combine them to create the induced orientational anisotropy decay function, R(t) (Eq. 1.3, reproduced here for clarity).

$$R(t) = \frac{I_{\|}(t) - I_{\perp}(t)}{I_{\|}(t) + 2I_{\perp}(t)} \qquad [1.3]$$

And R(t) is related to the motion and extent of confinement of the chromophore, (Eqs. 1.8 and 1.9 reproduced here for clarity).

$$R(t) = R(\infty) + (R(0) - R(\infty))\exp(-t/\tau_{HR})$$

$$\cos\theta_0 = 0.5\left(8\left(\frac{R(\infty)}{R(0)}\right)^{1/2} + 1\right)^{1/2} - 0.5 \qquad [1.8, 1.9]$$

$$\tau_{HR} = \frac{7\theta_0^2}{24D_w}$$

Where R(0) is the zero-time anisotropy, related to the angle between the excited and emitting transition dipole moments, R(∞) is the infinite time anisotropy, which is determined by the extent to which the chromophore motion is restricted by its local environment, θ_0 is the cone semi-angle in which the chromophore is able to reorient and D_w is the "wobbling" diffusion constant, which describes the motion of the chromophore about its tethering bond.[21,22] In this

model, the anisotropy decays as a single exponential. For free rotors, the anisotropy decay can exhibit up to five exponential decay components, depending on the axes of excitation and emission and on the shape of the volume swept out by the rotating species.[30] The observation of a multi-component decay in a homogeneous medium is not consistent with the hindered rotor model, owing to the tethering of the chromophore precluding facile rotational motion about more than the tethering axis. For the anisotropy decay data reported here we observe a two-component anisotropy decay and we assert that this two-component decay reflects two distinct chromophore populations that do not exchange population on the time scale of the measurement. For a heterogeneous system this is feasible and we note that the heterogeneity is not resolvable optically using our anisotropy imaging instrumentation.

While the pH and ionic strength dependencies of the tethered chromophore anisotropy decay dynamics are different, and their functional forms are expected (*vide infra*). It is important to consider that for both data sets the fast anisotropy decay component (*ca*. 300 ps) is consistent with the chromophore experiencing an environment that is slightly more resistive to rotational motion than water.[31] As would be expected if this is the case, changes in the overlayer pH and/or ionic strength should give rise to only small changes in the fast decay time component. The slow decay component, however, requires further consideration. The first issue is that the slow decay time constant is consistent with an environment that is much more viscous than water. Such data suggest that the chromophore population exhibiting a long anisotropy decay time does so because of interactions with the polar glycerol region of the lipid bilayer structure. While the nonpolar acyl chain region may well exhibit high local viscosity due to chain-chain interactions, the polarity of the rhodamine chromophore precludes significant direct interaction with this region of the bilayer.

To interpret the anisotropy decay imaging (FADI) data, determining the confining cone angle is essential, requiring the quantitative measurement of R(0) and R(∞) (Eqs. 2). The imaging instrument used to acquire the FADI data is optimized for spatially resolved data acquisition, but not for the quantitation of polarized emission transient absolute intensities. To evaluate the zero- and infinite-time anisotropies for our bilayer structures, we have constructed the same bilayer systems as an aqueous suspension of 50 - 100 nm diameter vesicles.[24] In this structural motif, we acquire anisotropy decay data using a TCSPC instrument capable of quantitating the relative intensities of polarized emission transients.[23] We extract R(0) and R(∞) from these experimental data and apply those results to the analysis of R(t) for the planar supported bilayers.

From these R(0) and R(∞) data for vesicles we extract a single anisotropy decay time constant, in contrast to the observed two component decay for planar bilayers, and calculate a cone angle (Eq. 2) of $\theta_0 \sim 90°$ for all ionic strength and pH measurements. The implications of these results are significant and can be understood as follows. For the planar bilayers, the fast anisotropy decay data we expect the bilayer structure to exhibit a random orientational distribution of local environments, giving rise to R(∞) ~ 0.08, and for the slow anisotropy decay data, where the chromophore interacts strongly with the bilayer headgroup, we could reasonably expect R(0) ~ 0, corresponding to $\theta_0 \sim 90°$. For such a two-population system, we would expect to recover a value of R(∞) that is the weighted average of that for the two distributions, and given the S/N ratio of our R(t) data, it is not likely that we could distinguish such an average value from its component values. The R(∞) data acquired for vesicles are thus consistent with our observation of a two-component population distribution where population exchange between the two components is facile (*vide infra*). Under the assumption that θ_0 for the fast decay

component is *ca*. 55° and for the slow decay component θ_0 is 90°, we can evaluate the fractional contribution of each component to the experimental data for the vesicles. For the planar bilayers we extract values for the wobbling diffusion constant for each population. This information provides insight into the local environment(s) as functions of pH (Table 3.1, Fig. 3.3a) and ionic strength (Table 3.2, Fig. 3.4a). Using these values for D_w, we take the vesicle decay time constant (Tables 3.3 and 3.4) as the weighted average of the time constants for each component, and thus determine the fractional contribution of each (Fig. 3.5). We consider these results in detail below.

pH	$A_1 \pm 1\sigma$	$\tau_1 \pm 1\sigma$ (ps)	$D_w \pm 1\sigma$ (MHz)	$A_2 \pm 1\sigma$	$\tau_2 \pm 1\sigma$ (ps)	$D_w \pm 1\sigma$ (MHz)
4	0.039 ± 0.007 (43±9%)	300 ± 26	896 ± 78	0.051 ± 0.005 (57±9%)	1603 ± 160	449 ± 46
5	0.036 ± 0.006 (40±9%)	339 ± 20	793 ± 43	0.053 ± 0.011 (60±9%)	2022 ± 123	356 ± 21
6	0.021 ± 0.005 (36±11%)	262 ± 37	1026 ± 145	0.038 ± 0.010 (64±11%)	2344 ± 202	308 ± 27
7	0.053 ± 0.009 (45±9%)	378 ± 45	711 ± 85	0.065 ± 0.005 (55±9%)	2760 ± 157	260 ± 16
8	0.064 ± 0.017 (49±15%)	389 ± 55	691 ± 98	0.066 ± 0.011 (51±15%)	2836 ± 224	254 ± 19
9	0.065 ± 0.007 (45±6%)	302 ± 38	890 ± 112	0.081 ± 0.011 (55±6%)	2421 ± 170	297 ± 21
10	0.036 ± 0.009 (44±14%)	360 ± 37	747 ± 77	0.046 ± 0.012 (56±14%)	2107 ± 137	343 ± 21

Table 3.1 Anisotropy decay time constant for SR-DOPE as a function of pH at constant ionic strength (I = 0.05) in planar bilayer structures. As discussed in the text, for the fast time constant, τ_1, $\theta_0 = 55°$ and for the slow time constant, τ_2, $\theta_0 = 90°$. Anisotropy decay data were best fit by a two-component exponential decay, $f(t) = A_1\exp(-t/\tau_1) + A_2\exp(-t/\tau_2)$.

Ionic Strength	$A_1 \pm 1\sigma$	$\tau_1 \pm 1\sigma$ (ps)	$D_w \pm 1\sigma$ (MHz)	$A_2 \pm 1\sigma$	$\tau_2 \pm 1\sigma$ (ps)	$D_w \pm 1\sigma$ (MHz)
0.05	0.063 ± 0.005 (77±9%)	323 ± 29	832 ± 75	0.019 ± 0.004 (23±9%)	2781 ± 164	260 ± 16
0.10	0.046 ± 0.011 (77±24%)	336 ± 53	800 ± 126	0.014 ± 0.004 (23±24%)	2528 ± 177	284 ± 19
0.20	0.040 ± 0.010 (73±23%)	254 ± 54	1058 ± 225	0.015 ± 0.003 (27±23%)	2191 ± 222	329 ± 32
0.30	0.041 ± 0.003 (68±8%)	242 ± 32	1111 ± 147	0.019 ± 0.004 (32±8%)	1709 ± 124	420 ± 29
0.40	0.045 ± 0.006 (66±13%)	209 ± 27	1286 ± 166	0.023 ± 0.007 (34±13%)	1407 ± 195	511 ± 70

Table 3.2 Anisotropy decay time constant for SR-DOPE as a function of ionic strength at constant pH (pH = 7) in planar bilayer structures. As discussed in the text, for the fast time constant, τ_1, $\theta_0 = 55°$ and for the slow time constant, τ_2, $\theta_0 = 90°$. Anisotropy decay data were best fit by a two-component exponential decay, $f(t) = A_1\exp(-t/\tau_1) + A_2\exp(-t/\tau_2)$.

pH	$\tau_{HR} \pm 1\sigma$ (ps)	X_{fast} (%)	X_{slow} (%)
4	1126 ± 114	37±12	63±12
5	1221 ± 47	48±5	52±5
6	1063 ± 18	62±4	38±4
7	1178 ± 64	66±4	34±4
8	1306 ± 68	63±5	37±5
9	1242 ± 49	56±5	44±5
10	1231 ± 66	50±6	50±6

Table 3.3 Anisotropy decay time constant for SR-DOPE as a function of pH at constant ionic strength (I = 0.05) in 50 nm diameter vesicles. Anisotropy decay data were best fit by a one-component exponential decay, $f(t) = A_1\exp(-t/\tau_{HR})$.

I	$\tau_{HR} \pm 1\sigma$ (ps)	X_{fast} (%)	X_{slow} (%)
0.05	1239 ± 37	63±3	37±3
0.1	1037 ± 47	68±4	32±4
0.2	1047 ± 89	59±7	41±7
0.3	1004 ± 14	48±5	52±5
0.4	1060 ± 83	29±14	71±14

Table 3.4 Anisotropy decay time constant for SR-DOPE as a function of ionic strength at constant pH (pH = 7) in vesicles. Anisotropy decay data were best fit by a one-component exponential decay, $f(t) = A_1\exp(-t/\tau_{HR})$. Using (Eqs. 2) the cone angle (θ_0) and diffusion constant (D_w) were calculated

It is important to note that we extracted $R(\infty)$ data from vesicles of the same composition as those used for the creation of the supported bilayer, but with a characteristic diameter of ca. 50 nm. For systems characterized by significant curvature, it is reasonable to expect morphology that is similar to that seen for a planar bilayer, but characterized by more facile exchange dynamics because of the structural freedom available to constituents of the bilayer leaflets.32 This expectation is realized for the system examined here. For the planar bilayer structure we are able to resolve discrete populations of chromophore that do not exchange on the timescale of the chromophore motion, while for vesicles we observe a single exponential decay time constant that is the weighted average of the two time constants seen for the planar bilayer. It is useful to compare the fraction of each chromophore population for the vesicles to the corresponding data for the supported planar bilayer. As noted above, we use the fast and slow time constants from the supported planar bilayer to extract the fractional contribution of each

to the weighted average for the vesicles. The relative fraction of the fast and slow chromophore populations depends differently on pH (Fig. 3.3b, Table 2.1) and ionic strength (Fig. 3.4b, Table 3.2) for the planar supported bilayers and vesicles (Fig. 3.5, Tables 3.3 and 3.4). The different dependencies provide some insight into the factors at play in mediating bilayer organization. For the planar supported bilayers, the diffusion constants depend on pH and ionic strength, but the fractional contributions of the two chromophore populations do not change with either pH or ionic strength (Figs. 3.3 and 3.4), within the uncertainty of the measurements. This result stands in contrast to the data for vesicles (Fig. 3.5), where the fractional contributions of the two chromophore populations change with both ionic strength and pH.

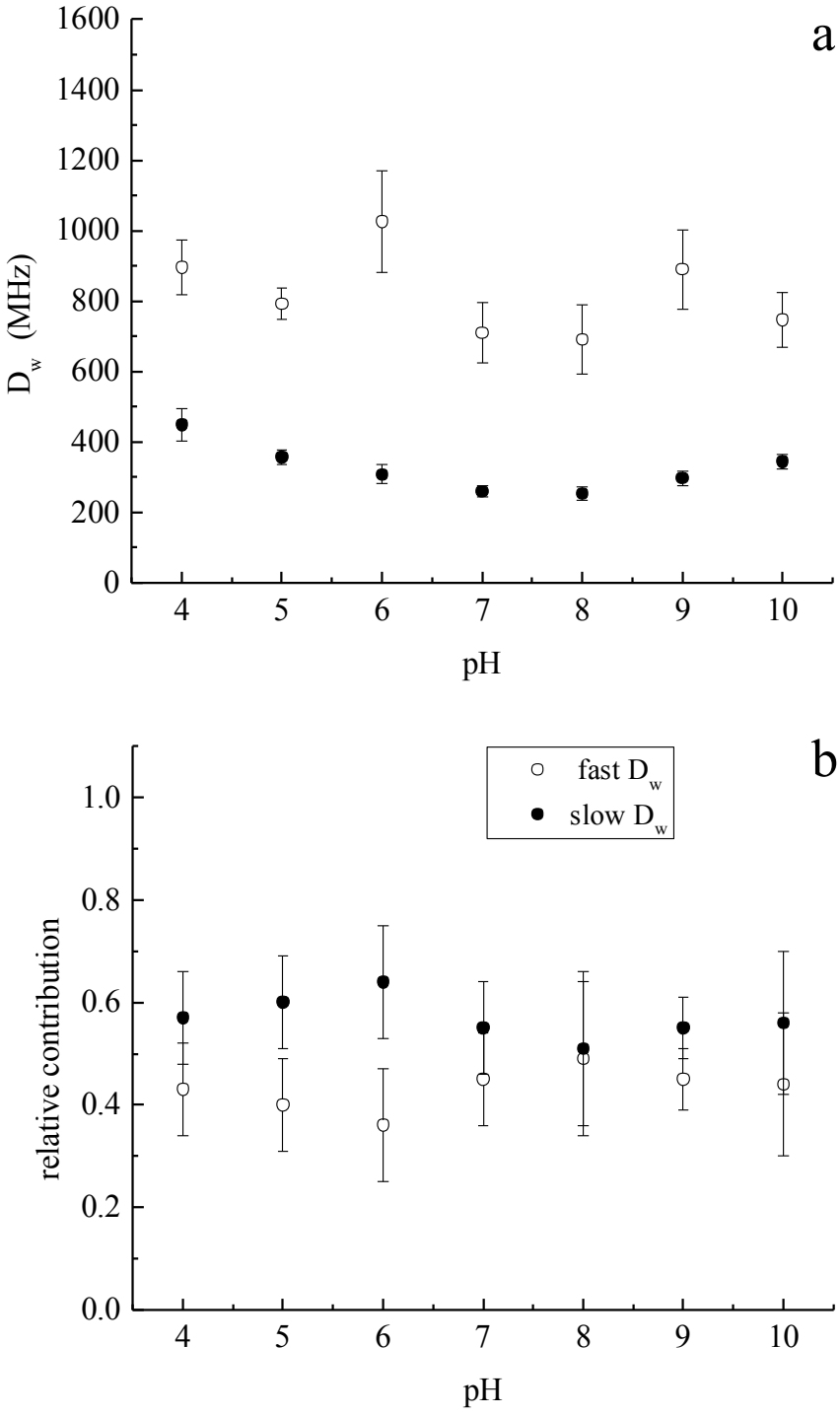

Figure 3.3 (a). Wobbling diffusion constant, D_w, as a function of pH, for the two resolved chromophore populations in planar supported bilayers. (b) Fractional contribution of each anisotropy decay component.

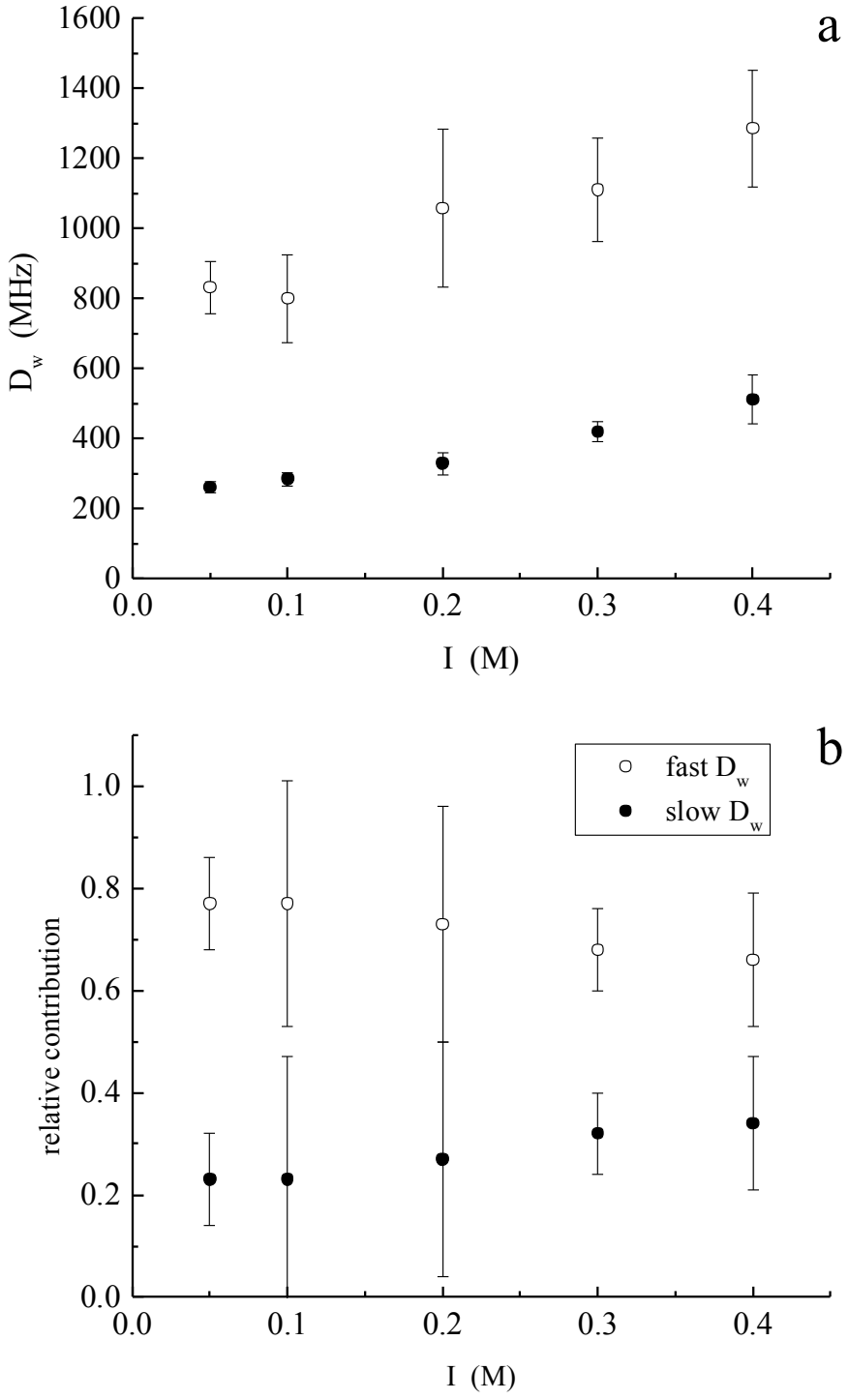

Figure 3.4 (a). Wobbling diffusion constant, D_w, as a function of ionic strength, for the two resolved chromophore populations in planar supported bilayers. (b) Fractional contribution of each anisotropy decay component.

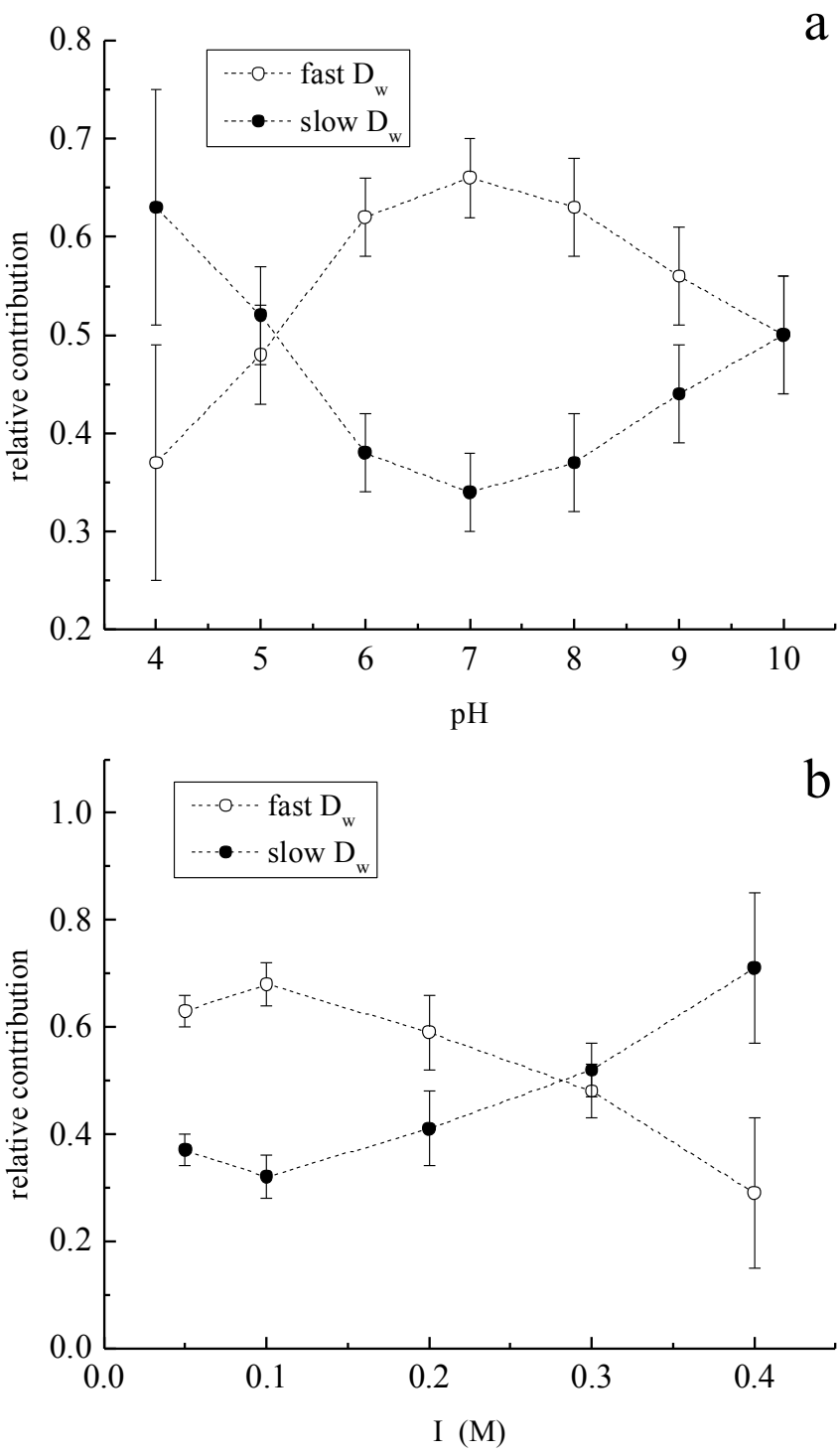

Figure 3.5 Relative fractional contribution of each anisotropy decay component as a function of pH (a) and ionic strength (b) for vesicles.

One structural difference between planar supported bilayers and vesicles is that the vesicle bilayer exhibits significant curvature, as noted above, which plays some role in mediating the facile exchange between the two chromophore populations.[33] Another structural difference has to do with pH and ionic strength gradients that can exist across the bilayer for the two structural motifs. For the planar supported bilayer, the (silica) surface on which the bilayer is supported is negatively charged and for the vesicle, the solution contained within it is nominally the same as that in which the vesicles reside. Thus there is not an environmental gradient across the bilayer comprising the vesicles, whereas there is an environmental gradient for planar bilayer layers. The (weak) adhesion to the support and the existence of a charge gradient across the bilayer could both serve to minimize lateral mobility within the bilayer. Indeed, this situation is not without parallel in mammalian plasma membranes, where membrane stiffness is influenced by the cytoskeleton.[34-37] For the vesicles, where there is neither a charge or mobility gradient across the bilayer, there are no analogous impediments to molecular motion in the plane of the bilayer. As such, translational diffusion within the vesicle bilayer is more facile, leading to the observed single exponential anisotropy decay. As the bilayer headgroups are screened by increasing ionic charge, or their extent of protonation varies, it would be reasonable to expect changes in the fractional contribution of the fast and slow processes, as is seen experimentally. We consider next the basis for the pH and ionic-strength dependence of the anisotropy decay data.

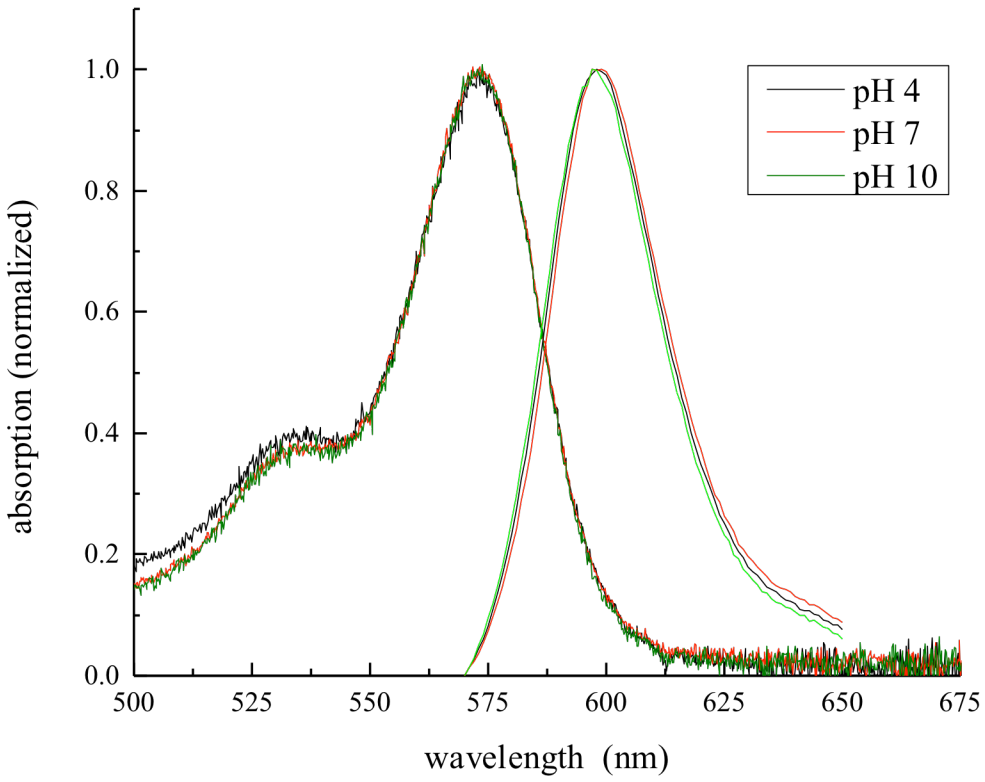

Figure 3.6 Normalized absorbance and emission spectra of SR-DOPE as a function of solution pH. These data were acquired for solutions at the pH values indicated.

The pH-dependent data were acquired at a fixed overlayer ionic strength of I = 0.05 (Table 1). The data show that the slow anisotropy decay time constant reaches a maximum of 2.8 ns in the pH 7-8 range and then decreases to 1.6 ns at pH 4 and to 2.1 ns at pH 10. We believe that the pH dependence is associated with changes in the bilayer headgroup local environment rather than any change in the chromophore; no pH-dependent spectral changes are seen for the rhodamine chromophore over this pH range (Fig. 3.6).

The three species contained in the bilayer are phosphocholine, sphingomyelin, and cholesterol, each of which has functionalities that undergo protonation/deprotonation equilibria. We can understand possible reasons for these effects based on the chemical structures of the

bilayer constituents (Fig. 3.1). At low pH the phosphocholine headgroup, which is typically depicted as zwitterionic, is expected to contain a protonated phosphate functionality and thus be cationic. Cholesterol has a $pK_a > 15$,[38] and for our experimental conditions is not expected to exhibit any change of protonation. Sphingomyelin contains alcohol and amide protons, with pK_as in the region of 18 and 26, respectively.[18] As a consequence, these labile protons are not expected to play a significant role in the pH dependence we observe. However, the sphingomyelin phosphate functionality is expected to participate in acid-base equilibria analogous to that for phosphocholine over the pH range of our experiments. For all pH values examined here, the phosphocholine and sphingomyelin phosphate moieties thus mediate the pH-dependent organization of the system. Near pH 7 the zwitterionic nature of the lipid headgroups can exhibit significant intermolecular charge-based interactions, leading to changes in the ability of the chromophore to execute rotational motion. For low pH, the phosphate head groups are protonated, giving rise to charge repulsion between the phosphate headgroups, and consequently greater freedom of motion for the chromophore. For high pH conditions, sufficient OH^- will be present in solution to associate with choline headgroup moieties, leaving anionic repulsion between the phosphate headgroup functionalities to produce a result at least somewhat analogous to that seen for low pH conditions. We expect the change in extent of protonation in the bilayer constituents will alter the (cholesterol) domain sizes in the supported bilayers, and this situation is realized experimentally (Fig. 3.2). There are other factors that can and do affect the domain structure of these films, and we consider some of them below.

The dependence of the chromophore anisotropy decay time on overlayer ionic strength is different than the pH-dependence. The dependence on ionic strength is monotonic, with the slow anisotropy decay time constant ranging from 2.75 ns at I = 0.05 to 1.4 ns at I = 0.4. We attribute

this trend to the increasing extent of charge compensation and screening in the bilayer with increasing ionic strength, leading to a reduction in the overall energy of intermolecular interactions between bilayer constituents and thus an environment that provides progressively less constraint on the motional freedom of the tethered chromophore. We note that, as with the pH-dependence, changes in ionic strength are expected to alter the organization of the bilayer because of the effect on intermolecular interactions within the bilayer headgroup region.

The above discussion focuses on protonation/deprotonation and charge compensation/screening of the phospholipid species in the bilayer. The rhodamine chromophore is cationic and it is tethered to a phospholipid by means of an amino functionality, which can participate in protonation/deprotonation equilibria. Thus the probe is potentially involved in at least some of the changes associated with pH and ionic strength. We have found no evidence for dissociation of the probe from its tethering phosphoethanolamine moiety, however, and as noted above, the chromophore exhibits no spectral changes over the pH region of 4-10. Whatever roles the chromophore charge or tethering bond play in the observed dynamics do not appear to play a significant role in the changes we observe.

As noted above, we observe both microscopic and macroscopic changes in the morphology of our phase-segregated supported bilayers as a function of pH and ionic strength. For the planar supported bilayers, there are nine distinct interactions that play a role in mediating bilayer morphology; cholesterol-mica, phosphocholine-mica, sphingomyelin-mica, cholesterol-phosphocholine, cholesterol-sphingomyelin, phosphocholine-sphingomyelin, cholesterol-overlayer, sphingomyelin-overlayer, and phosphocholine-overlayer. While it is not feasible to distinguish the contributions of each interaction given the data we report here, the dominant changes in interactions we probe for the planar supported bilayer are those between the aqueous

overlayer and the bilayer constituents. Differences in our results for the unilamellar vesicles and planar supported bilayers reflect the absence or presence of interactions between the bilayer constituents and the mica support. The issue of how the change in overlayer properties (pH and ionic strength) influences the mica support remains unresolved because the permeability of the bilayer has not been evaluated. If the time-resolved spectroscopic results for bilayers supported on ITO are similar to those reported here, it may be possible to gauge the permeability of the bilayer through electrochemical studies.

Conclusions

Synthetic supported bilayer structures are important to a number of applications ranging from the creation of biomimetic interfaces to the hosting of transmembrane proteins for chemical sensing applications. Understanding the relationship between supported bilayer morphology and its environment is a key issue in determining the utility of any specific system. The morphology of such supported bilayers represents the global minimization of the interactions between the bilayer constituents, the support and the overlayer in contact with the bilayer. While this is true for both planar supported bilayers and for vesicles, there is a discernible difference in the mobility and dynamics of species incorporated into these two bilayer structures because of bilayer curvature and the inner leaflet being in contact with a liquid versus a solid. By varying overlayer pH and ionic strength, we can exert systematic change on three of the nine interfaces in our ternary supported planar bilayers. Using a headgroup-tethered chromophore to probe the interface with the aqueous overlayer, we have found that its anisotropy decay dynamics are sensitive to the overlayer properties. We understand these effects in the context of protonation/deprotonation equilibria or charge screening effects, providing us with a facile means of controlling bilayer morphology.

REFERENCES

REFERENCES

1. Ingle, J. D.; Crouch, S. R. *Spectrochemical Analysis*; Prentice Hall: Upper Saddle River, NJ, 1988.

2. Bard, A. J.; Faulkner, L. R. *Electrochemical Methods Fundamentals and Applications, Second Edition*; John Wiley & Sons, Inc.: New York, Chichester, Weinheim, Brisbane, Singapore, Toronto, 2001.

3. Fhaner, C. J.; Liu, S.; Ji, H.; Simpson, R. J.; Reid, G. E. Comprehensive Lipidome Profiling of Isogenic Primary and Metastatic Colon Adenocarcinoma Cell Lines. *Anal. Chem.* **2012**, *84*, 8917-8926.

4. Brian, A. A.; McConnell, H. M. Allogenic Stimulation of Cytotoxic T Cells by Supported Planar Membranes. *Proc. Nat. Acad. Sci. USA* **1984**, *81*, 6159-6163.

5. Tamm, L. K.; McConnell, H. M. Supported Phospholipid Bilayers. *Biophys. J.* **1985**, *47*, 105-113.

6. Dominska, M.; Krysinski, P.; Blanchard, G. J. Interrogating Interfacial Organization in Planar Bilayer Structures. *Langmuir* **2008**, *24*, 8785-8793.

7. Greenough, K. P.; Blanchard, G. J. Lipid Headgroups Mediate Organization and Dynamics in Bilayers. *Spectrochimica Acta Part a-Molecular and Biomolecular Spectroscopy* **2009**, *71*, 2050-2056.

8. Greiner, A. J.; Pillman, H. A.; Worden, R. M.; Blanchard, G. J.; Ofoli, R. Y. Effect of Hydrogen Bonding on the Rotational and Translational Dynamics of a Headgroup-Bound Chromophore in Bilayer Lipid Membranes. *Journal of Physical Chemistry B* **2009**, *113*, 13263-13268.

9. Lapinski, M. M.; Blanchard, G. J. The Role of Phospholipid Headgroups in Mediating Bilayer Organization Perturbations Induced by the Presence of a Tethered Chromophore. *Chemistry and Physics of Lipids* **2007**, *150*, 12-21.

10. Pillman, H. A.; Blanchard, G. J. Effects of Ethanol on the Organization of Phosphocholine Lipid Bilayers. *Journal of Physical Chemistry B* **2010**, *114*, 3840-3846.

11. Setiawan, I.; Blanchard, G. J. Structural Disruption of Phospholipid Bilayers over a Range of Length Scales by N-Butanol. *Journal of Physical Chemistry B* **2014**, *118*, 3085-3093.

12. Setiawan, I.; Blanchard, G. J. Ethanol-Induced Perturbations to Planar Lipid Bilayer Structures. *Journal of Physical Chemistry B* **2014**, *118*, 537-546.

13. Crane, J. M.; Tamm, L. K. Fluorescence Microscopy to Study Domains in Supported Lipid Bilayers. *Methods in Molecular Biology* **2007**, *400*, 481-488.

14. Kiessling, V.; Wan, C.; Tamm, L. K. Domain Coupling in Asymmetric Lipid Bilayers. *Biochimica et Biophysica Acta* **2009**, *1788*, 64-71.

15. Maloney, K. M.; Grainger, D. W. Phase Separated Anionic Domains in Ternary Mixed Lipid Monolayers at the Air-Water Interface. *Chemistry and Physics of Lipids* **1993**, *65*, 31-42.

16. McKiernan, A. E.; Ratto, T. V.; Longo, M. L. Domain Growth, Shapes and Topology in Cationic Lipid Bilayers on Mica by Fluorescence and Atomic Force Microscopy. *Biophys. J.* **2000**, *79*, 2605-2615.

17. Mulder, W. H. Equilibrium Size Distributions of Circular Domains in Amphiphilic Monolayers. *Journal of Physical Chemistry B* **1997**, *101*, 7744-7750.

18. Samsonov, A. V.; IMihalyov, I.; Cohen, F. S. Characterization of Cholesterol-Sphingomyelin Domains and Their Dynamics in Bilayer Membranes. *Biophys. J.* **2001**, *81*, 1486-1500.

19. Lee, D. W.; Min, Y.; Dhar, P.; Ramachandran, A.; Israelachvili, J. N.; Zasadzinski, J. A. Relating Domain Size Distribution to Line Tension and Molecular Dipole Density in Model Cytoplasmic Myelin Lipid Monolayers. *Proc. Nat. Acad. Sci. USA* **2011**, *108*, 9425-9430.

20. Benvegnu, D. J.; McConnell, H. M. Line Tension between Liquid Domains in Lipid Monolayers. *Journal of Physical Chemistry* **1992**, *96*, 6820-6824.

21. Lipari, G.; Szabo, A. Effect of Librational Motion on Fluorescence Depolarization and Nuclear Magnetic Resonance Relaxation in Macromolecules and Membranes. *Biophys. J.* **1980**, *30*, 489-506.

22. Szabo, A. Theory of Fluorescence Depolarization in Macromolecules and Membranes. *J. Chem. Phys.* **1984**, *81*, 150-167.

23. Pillman, H. A.; Blanchard, G. J. Effects of Energy Dissipation on Motional Dynamics in Unilamellar Vesicles. *J. Phys. Chem. B* **2010**, *114*, 13703-13709.

24. Lapinski, M. M.; Castro-Forero, A.; Greiner, A. J.; Ofoli, R. Y.; Blanchard, G. J. A Comparison of Liposomes Formed by Sonication and Extrusion: Rotational and Translational Diffusion of an Imbedded Chromophore. *Langmuir* **2007**, *23*, 11677-11683.

25. Dutta, P.; Sen, P.; Mukherjee, S.; Bhattacharyya, K. Solvation Dynamics in Dmpc Vesicle in the Presence of a Protein. *Chemical Physics Letters* **2003**, *382*, 426-433.

26. Garrison, M. D.; Potts, R. O.; Abraham, W. Frequency-Domain Fluorescence Spectroscopy of Human Stratum Corneum. *Proceedings of SPIE* **1994**, *2137*, 725.

27. Nipper, M. E.; Majd, S.; Mayer, M.; Lee, J. C. M.; Theodorakis, E. A.; Haidekker, M. A. Characterization of Changes in the Viscosity of Lipid Membranes with the Molecular Rotor Fcvj. *Biochimica et Biophysica Acta - Biomembranes* **2008**, *1778*, 1148-1153.

28. Chan, S. I.; Seiter, C. H. A.; Feigenson, G. W. Anisotropic and Restricted Molecular Motion in Lecithin Bilayers. *Biochemical and Biophysical Research Communications* **1972**, *46*, 1488-1492.

29. Gally, H. U.; Niederberger, W.; Seelig, J. Conformation and Motion of the Choline Head Group in Bilayers of Dipalmitoyl-3-Sn-Phosphatidylcholine. *Biochemistry* **1975**, *14*, 3647-3652.

30. Chuang, T. J.; Eisenthal, K. B. Theory of Fluorescence Depolarization by Anisotropic Rotational Diffusion. *J. Chem. Phys.* **1972**, *57*, 5094-5097.

31. Debye, P. *Polar Molecules* Chemical Catalog Co.: New York 1929.

32. Lapinski, M. M.; Blanchard, G. J. Interrogating the Role of Liposome Size in Mediating the Dynamics of a Chromophore in the Acyl Chain Region of a Phospholipid Bilayer. *Chemistry and Physics of Lipids* **2008**, *153*, 130-137.

33. Baumgart, T.; Hess, S. T.; Webb, W. W. Imaging Coexisting Fluid Domains in Biomembrane Models Coupling Curvature and Line Tension. *Nature* **2003**, *425*, 821-824.

34. Yeung, T.; Georges, P. C.; Flanagan, L. A.; Marg, B.; Ortiz, M.; Funaki, M.; Zahir, N.; Ming, W.; Weaver, V.; Janmey, P. A. Effects of Substrate Stiffness on Cell Morphology, Cytoskeletal Structure and Adhesion. *Cell Mot. Cytoskel.* **2005**, *60*, 24-34.

35. Wang, N.; Butler, J. P.; Ingber, D. E. Mechanotransduction across the Cell Surface and through the Cytoskeleton. *Science* **1993**, *260*, 1124-1127.

36. Maniotis, A. J.; Chen, C. S.; Ingber, D. E. Demonstration of Mechanical Connections between Integrins, Cytoskeletal Filaments, and Nucleoplasm That Stabilize Nuclear Structure. *Proc. Nat. Acad. Sci. USA* **1997**, *94*, 849-854.

37. Byfield, F. J.; Aranda-Espinoza, H.; Romanenko, V. G.; Rothblat, G. H.; Levitan, I. Cholesterol Depletion Increases Membrane Stiffness of Aortic Endothelial Cells. *Biophys. J.* **2004**, *87*, 3336-3343.

38. Vrielink, A. *Cholesterol Oxidase: Structure and Function*; Springer: Dordrecht, Heidelberg, London, New York, 2010; Vol. 51.

CHAPTER 4

Conclusions

Time correlated single photon counting detection (TCSPC) detection is a very useful technique which gives us the ability to extract information on intermolecular interactions and energy transfer for free rotors in solution and for tethered chromophores in supported bilayer structures. Studying the excitation energy-dependence of solution phase chromophores provides insight into transient heating and energy transfer processes of tetracene in *n*-alkanes C_8 through C_{16}. In the tetracene study, a laser system equipped with TCSPC detection was used and time-domain anisotropy decay data were collected for the $S_1 \leftarrow S_0$ excitation and for $S_2 \leftarrow S_0$ excitation of the chromophore. One of the first noticed things in this experiment was that reorientation time was independent of the solvent chain length for the S_2 state due to rapid relaxation from the S_2 state to the S_1 state. Secondly, for the $S_1 \leftarrow S_0$ excitation data the reorientation time had an odd-even effect, due to tetracene interactions with the alkane solvent terminal methyl groups.

Understanding the organization of these systems and how changes to the aqueous overlayer influence the rigidity of a model cell membrane could lead to the development of planar lipid bilayer biosensor. For the bilayer study, fluorescence anisotropy decay imaging(FADI) equipped with TCSPC detection was utilized to study the intermolecular interactions, organization, and dynamics of planar lipid bilayers. The purpose of this study was to gain a better understanding of how pH and ionic strength influence the model cell membranes on a mica substrate, for a next step of adding transmembrane proteins. In this study a rhodamine tethered phospholipid was included in the bilayer on the substrate and the rotational dynamics were assessed. It was found that there were two different environments, based on a two-

component decay. A faster decay independent of pH and ionic strength, and a slower decay dependent on both. From the slower decay, there were faster rotational constants at high and low pH values and slower time constants near neutral pH. These data are interpreted as follows; at neutral pH more molecular interactions are occurring so there is a more rigid environment, while at high and low pH fewer molecular interactions were occurring, resulting in environment where the wobbling tethered-chromophore reoriented much faster. In addition, as the ionic strength increased, the rotational time constant decreased, which was due to screening effects. This research has shown us that we have a means of controlling bilayer morphology based on protonation/deprotonation equilibria or charge screening effects. Subsequently, future work on this project would be focused on developing these systems further with the goal of creating a biosensor.